Redox Biology 71 (2024) 103104

Contents lists available at ScienceDirect

Redox Biology

journal homepage: www.elsevier.com/locate/redox

Inhibition of MST1 ameliorates neuronal apoptosis via GSK3β/β-TrCP/NRF2 pathway in spinal cord injury accompanied by diabetes

Weijun Huang [a,b,c,1], Depeng Wu [a,b,c,1], Chaoyang Cai [a,b,c,1], Hui Yao [a], Zhenming Tian [a,b,c], Yang Yang [a,b,c], Mao Pang [a,b,c], Limin Rong [a,b,c,**], Bin Liu [a,b,c,*]

[a] Department of Spine Surgery, The Third Affiliated Hospital of Sun Yat-sen University, Guangzhou, PR China
[b] Guangdong Provincial Center for Quality Control of Minimally Invasive Spine Surgery, Guangzhou, PR China
[c] Guangdong Provincial Center for Engineering and Technology Research of Minimally Invasive Spine Surgery, Guangzhou, PR China

ARTICLE INFO

Keywords:
Spinal cord injury (SCI)
Diabetes
Mammalian sterile20-like kinase (MST1)
Oxidative stress
Nuclear factor erythroid 2-related factor 2 (NRF2)

ABSTRACT

Aims: Spinal cord injury (SCI) is a devastating neurological disease that often results in tremendous loss of motor function. Increasing evidence demonstrates that diabetes worsens outcomes for patients with SCI due to the higher levels of neuronal oxidative stress. Mammalian sterile 20-like kinase (MST1) is a key mediator of oxidative stress in the central nervous system; however, the mechanism of its action in SCI is still not clear. Here, we investigated the role of MST1 activation in induced neuronal oxidative stress in patients with both SCI and diabetes.

Methods: Diabetes was established in mice by diet induction combined with intraperitoneal injection of streptozotocin (STZ). SCI was performed at T10 level through weight dropping. Advanced glycation end products (AGEs) were applied to mimic diabetic conditions in PC12 cell line in vitro. We employed HE, Nissl staining, footprint assessment and Basso mouse scale to evaluate functional recovery after SCI. Moreover, immunoblotting, qPCR, immunofluorescence and protein-protein docking analysis were used to detect the mechanism.

Results: Regarding in vivo experiments, diabetes resulted in up-regulation of MST1, excessive neuronal apoptosis and weakened motor function in SCI mice. Furthermore, diabetes impeded NRF2-mediated antioxidant defense of neurons in the damaged spinal cord. Treatment with AAV-siMST1 could restore antioxidant properties of neurons to facilitate reactive oxygen species (ROS) clearance, which subsequently promoted neuronal survival to improve locomotor function recovery. *In vitro* model found that AGEs worsened mitochondrial dysfunction and increased cellular oxidative stress. While MST1 inhibition through the chemical inhibitor XMU-MP-1 or MST1-shRNA infection restored NRF2 nuclear accumulation and its transcription of downstream antioxidant enzymes, therefore preventing ROS generation. However, these antioxidant effects were reversed by NRF2 knockdown. Our in-depth studies showed that over-activation of MST1 in diabetes directly hindered the neuroprotective AKT1, and subsequently fostered NRF2 ubiquitination and degradation via the GSK3β/β-TrCP pathway.

Conclusion: MST1 inhibition significantly restores neurological function in SCI mice with preexisting diabetes, which is largely attributed to the activation of antioxidant properties via the GSK3β(Ser 9)/β-TrCP/NRF2 pathway. MST1 may be a promising pharmacological target for the effective treatment of spinal cord injury patients with diabetes.

1. Introduction

Spinal cord injury (SCI) can disrupt the pathways projecting from the brain and brainstem to the lumbar spinal cord, causing severe motor, sensory, and autonomic dysfunction [1,2]. The pathophysiology of SCI is divided into acute, sub-acute and chronic phases. The acute phase of SCI is characterized by ion imbalance, generation of free radicals, lipid peroxidation, and inflammation. When acute injury persists, the sub-acute phase begins, marked by neuronal apoptosis, axonal

* Corresponding author. Department of Spine Surgery, The Third Affiliated Hospital of Sun, Yat-Sen University, Guangzhou, 510630, PR China.
** Corresponding author. Department of Spine Surgery, The Third Affiliated Hospital of Sun, Yat-Sen University, Guangzhou, 510630, PR China.
E-mail addresses: ronglm@mail.sysu.edu.cn (L. Rong), liubin6@mail.sysu.edu.cn (B. Liu).
[1] These authors contributed equally to the study.

https://doi.org/10.1016/j.redox.2024.103104
Received 22 December 2023; Received in revised form 8 February 2024; Accepted 23 February 2024
Available online 28 February 2024

Abbreviations

SCI	spinal cord injury
DM	diabetes mellitus
MST1	mammalian sterile20-like kinase 1
NRF2	nuclear factor erythroid 2-related factor 2
ROS	Reactive oxygen species
GSK3β	glycogen synthase kinase 3β
β-TrCP	β-transducin repeat-containing protein
SOD2	superoxide Dismutase 2
NQO1	NADPH quinone dehydrogenase 1
HO1	heme oxygenase 1
Keap1	kelch-like ECH associated protein 1
ROS	reactive oxygen species
RNS	reactive nitrogen species
GSR	glutathione reductase
STZ	streptozotocin
AAV	adeno-associated virus
TUNEL	terminal deoxynucleotidyl transferase-mediated dUTP nick end labeling
NEUN	neuron-specific nuclear protein
NF200	neurofilament protein 200
Tomm20	mitochondrial 20 kDa outer membrane protein
Drp1	dynamin-related protein 1
MDA	malondialdehyde
GSH	glutathione
AGEs	advanced glycation end products
DHE	dihydroethidium
NOX2	NADPH oxidase 2
NOX4	NADPH oxidase 4
CytoC	cytochrome *c*
ARE	antioxidant response elements

demyelination, and the formation of glial scars. Besides, the chronic phase is manifested by features including the formation of cystic cavities and the maturation of neural glial scars [3]. Co-existing conditions, such as diabetes mellitus (DM) or high blood glucose levels, are prognostic factors for the poor outcomes of neurological disorders in humans [4–7]. Diabetes is a common and insidious metabolic disorder [8]. In cases of acute trauma, It is not rare to discover that patients have concurrent diabetes [9]. Spinal cord injury patients, experiencing prolonged bedridden, often exhibit an increased susceptibility to overweight and metabolic disturbances, thus they have also been reported to be at a higher risk of diabetes and hyperlipidemia [10]. In turn, increasing evidence has shown that DM plays a role in accelerating functional impairment in SCI, which could be attributed to neuroinflammation [4,11], autophagy [12], oxidative stress [13], and endoplasmic reticulum stress [14,15]. However, a comprehensive understanding of how diabetes exacerbates the pathological changes in SCI remains elusive.

Oxidative stress is a central process in SCI and represents an imbalance between ROS and RNS production and the capacity of the antioxidant defense system [16]. Previous studies have shown that mammalian sterile20-like kinase (MST1) mediates neuronal cell death and confers inflammatory impairment initiated by oxidative stress [17,18]. Furthermore, MST1 knockdown inhibits oxidative stress and neuronal damage during intracerebral haemorrhage [19]. A previous study demonstrated that the apoptosis-promoting kinase MST1 plays a crucial role in both neuronal cell death and microglial activation upon oxidative stress in mammalian primary neurons [17]. Based on the above evidence, MST1 may participate in the neural cell apoptosis caused by oxidative stress. In particular, MST1 is significantly upregulated in the nervous system under diabetogenic conditions, which augments oxidative stress and cognitive decline [20,21]. It was thus speculated that diabetes might exacerbate the pathological process of SCI by regulating MST1 expression.

Nuclear factor erythroid 2-related factor 2 (NRF2) is a key transcription factor involved in the cellular oxidative stress response [22]. In the cascade of oxidative stress reactions, NRF2 controls the expression of multiple endogenous antioxidant genes and phase II detoxifying enzymes, including NADPH quinone dehydrogenase 1 (NQO1), superoxide dismutase (SOD), heme oxygenase-1 (HO-1), glutathione reductase (GSR), glutathione *S*-transferase alpha (GSTA), and catalase (CAT) [23]. Numerous researchers have shown that NRF2 activation results in cytoprotection against various neurodegenerative diseases, such as amyotrophic lateral sclerosis (ALS), Alzheimer's, and Parkinson's diseases [24,25]. Moreover, strategies aimed at addressing SCI may involve the modulation of NRF2-regulatory pathways [26,27]. The expression of NRF2 and HO-1 is reportedly significantly upregulated in the early stages of SCI, thus increasing antioxidant levels [26]. Nevertheless, higher levels of oxidative stress markers and lower antioxidant marker activities have been observed in patients with diabetes [28]. Recently, NRF2 was recognized as a downstream mediator of MST1 in several disease models. For example, MST1 induces the progression of nasal inflammatory injury by repressing NRF2 [29]. Conversely, the suppression of MST1 activity could trigger autophagy and help stem cells survive H_2O_2-induced injury via the Keap1/NRF2 pathway [30]. Nevertheless, the precise mechanism has not been thoroughly investigated. It was thus hypothesized that the co-existence of diabetes impedes the adaptive antioxidant response of neurons in spinal cord injuries, and further investigation is required to determine whether this adverse effect is associated with diabetes-induced MST1 activation.

In this study, using both normal and diabetic mouse SCI models, a direct link was confirmed between the physiological changes in diabetes and the exacerbation of SCI outcomes and the treatment effects of MST1 depletion in terms of alleviating oxidative stress were explored. Furthermore, the underlying mechanisms of MST1 modulating antioxidants were investigated and a novel therapeutic target for impaired motor function following traumatic SCI exacerbated by prevalent metabolic disorders was identified.

2. Material and methods

2.1. Animals and treatments

All surgical procedures and postoperative care protocols were approved by the Animal Care and Use Committee of the Third Affiliated Hospital of Sun Yat-sen University (approval number: IACUC-F3-22-0720). The animals were housed in a specific pathogen-free facility under a 12:12-h light-dark cycle. Every possible measure was taken to minimize the number of animals used and alleviate any potential discomfort.

Six-week-old female C57BL/6 J mice, were allocated randomly to two distinct groups: the control group (n = 37) and the diabetes mellitus group (n = 66). The induction of type 2 diabetes was initiated with a 6-week high-fat, high-sucrose diet (HFD) regimen to induce insulin resistance. Subsequently, intraperitoneal injections of STZ (50 mg/kg body weight, dissolved in 0.1 mol/L citrate buffer [pH 4.5]) were administered daily for three consecutive days [31]. Two weeks after STZ injection, hyperglycaemia (defined as fasting blood glucose levels ≥250 mg/dL) was successfully induced. Mice in the control group were injected with an equivalent volume of vehicle solution. Subsequently, the control group mice were subdivided into sham (n = 17) or SCI groups (n = 20), and the diabetic mice were randomly allocated into three subgroups: DM + SCI, DM + SCI + Adeno-associated virus (AAV)-vehicle, and DM + SCI + AAV-shMST1 (n = 20 each). The

surgical procedure for inducing SCI was conducted two weeks after the STZ injection. First, the mice were anaesthetised by an intraperitoneal injection of sodium pentobarbital (40 mg/kg). Subsequently, laminectomy was performed at the T7–T9 level, and the exposed spinal cord was lesioned using an Infinite Horizon Impactor (Precision Systems and Instrumentation, LLC) to induce a moderate (70 kD) contusion. During the surgery, 1 μL of viral solution carrying AAV-vehicle or AAV-shMST1 was injected into the lesion site in the DM + SCI + AAV-vehicle and DM + SCI + AAV-shMST1 group, respectively. Following SCI, bladders were manually emptied twice daily until spontaneous voiding resumed. In the sham group, laminectomy was performed, but no SCI contusion was induced. Furthermore, an additional 12 female 6-week-old C57BL/6 J mice were purchased, and divided into two subgroups: one group was fed a normal diet for 6 weeks (control group, n = 6), and the other group was induced with type 2 diabetes using the aforementioned method (diabetes group, n = 6). These mice did not undergo any surgical procedures and were sacrificed to compare the physiological parameters between normal and diabetic mice. The experimental animal model procedures and group information are presented in Fig. 8A and Table S1.

2.2. AAV injection

AAV-siRNA-MST1, purchased from Obio Technology, was used to knock down MST1 in mice, with the AAV vehicle serving as a control. The target sequence for MST1-siRNA was CCAGGAATGTAACACGAAGTA. The AAV (1 μL) was administered into the lesion site (approximately 300 μm in vertical depth) using a 10-μL Hamilton syringe (Hamilton Co, USA) at a flow rate of 200 nL/min. Following injection, the needle was kept in place for 2 min before being slowly withdrawn.

2.3. Functional outcome measurement

The Basso Mouse Scale (BMS) score was assessed 0, 3, 7, 14, 21, and 28 days postoperation to evaluate hindlimb locomotor function. For the angle of the inclination test, the highest angle at which a rat could maintain its position on a rubber mat-covered board for 5 s without falling was recorded. Footprint analysis was conducted 28 days after injury. The front limbs were marked with blue dye, and the rear limbs with red dye. The movement of the mice was confined and they were encouraged to walk linearly to enable their stride length to be recorded.

2.4. Histology and immunohistochemistry staining

Coronal sections of spinal cord segments were fixed using 4% paraformaldehyde and subsequently embedded in paraffin. Paraffin-embedded sections were sliced (5 μm thick) and subjected to haematoxylin and eosin (H&E) and Nissl staining.

For immunohistochemical preparation, the sections were incubated with primary antibodies targeting pMST1 (phospho T183; 1:50; Ab79199; Abcam), NRF2(1:100; PA588084; Thermo), and SOD2 (1:200; 66474-1-IG; Proteintech) at 4 °C over-night. Subsequently, the sections were washed thrice with PBS and incubated with the respective secondary antibodies. The resulting reaction was visualized using DAB solution. After counterstaining with haematoxylin, the sections were examined under a light microscope (400 × magnification; Nikon, Tokyo, Japan).

2.5. Immunofluorescence and TUNEL staining

The spinal cord sections and PC12 cells fixed with 4% paraformaldehyde (PFA) were subjected to three washes with PBS. Subsequently, the sections were blocked with 10% goat serum in PBS for 1 h at room temperature and then incubated with the following antibodies overnight at 4 °C: NEUN (1:500; ab104224; Abcam), NRF2 (1:100; MA5-42371; Invitrogen), SOD2 (1:200; 66474-1-IG; Proteintech), NF200 (1:200; ab254348; Abcam), Tomm20 (1:200; 42,406; Cell Signaling Technology), Drp1 (1:100; 8570; Cell Signaling Technology), and HO1 (1:200; 66743-1-IG; Proteintech). Secondary antibodies, including goat anti-mouse IgG H&L (Alexa Fluor 488, ab6785, Abcam, USA), goat anti-mouse IgG H&L (Alexa Fluor 594, A32727, Thermo, USA), goat anti-rabbit IgG H&L (Alexa Fluor 488, A11070, Thermo, USA), and goat anti-rabbit IgG H&L (Alexa Fluor 594, #8889, CST, USA), were applied for 2 h at room temperature. Finally, the nuclei were stained with Hoechst 33,258 (Beyotime) at room temperature for 15 min. For TUNEL staining, the sections were cultured in a dark and humid environment at 37 °C for 2 h using the TUNEL Apoptosis Assay Kit (C1088, Beyotime) in accordance with the manufacturer's instructions. Images were captured using a Leica SP8 Lightning confocal microscope and light microscope (400× magnification; Nikon, Japan), and eight randomly chosen fields of view were selected for each sample.

2.6. Measurements of antioxidants and oxidative biomarkers

Spinal cord samples were collected and lysed with RIPA buffer 0, 14, and 28 days after the SCI. Following the protocols provided by the ELISA kits, the enzymatic activity of the catalase (S0051; Beyotime, China), and the levels of glutathione (GSH) (A006; Jiancheng Bioengineering Institute, China) and malondialdehyde (MDA) (S0131S; Beyotime, China) were evaluated.

2.7. Cell culture and drug application

The rat PC12 cell line was cultured in DMEM (Gibco, USA) supplemented with 10% fetal bovine serum (FBS, Gibco, USA) and 1% penicillin/streptomycin (Life Technologies, USA). Advanced glycation end products (AGEs), which are toxic compounds proposed as risk factors in the pathogenesis of diabetes, were applied to mimic the effects of diabetic conditions on the cells [32]. *Tert*-butyl hydroperoxide (TBHP) solution was used (Sigma-Aldrich, 458,139) as a mediator of oxidative damage. XMU-MP-1 (Y-100526, MedChemExpress) was dissolved in DMSO and applied at 5 μM for 6 h in PC12 to inhibit MST1 activity.

2.8. Transfection in PC12 cells

A lentivirus vector containing sequences encoding the rat MST1 gene (Lv-MST1) was generated by Cyagen Biosciences Inc. (USA) to overexpress MST1, and an empty lentivirus vector was used as a control (Lv-Ctrl). To knockdown MST1 expression in PC12 cells, the cells were transfected with lentiviruses containing shRNA against MST1 (MST1-shRNA) and scrambled shRNA. In addition, to silence NRF2 expression, PC12 cells were transiently transfected with NRF2 siRNA (Obio Technology, China) using the Lipofectamine™ 2000 Transfection Reagent (11668019, Thermo). The target sequences for the MST1 and NRF2 knockdown were as follows:

ShRNA-MST1: 5′-GGTATGGTTGGGTACAATTAACTCGAGTTAATTGTACCCAACCATACC-3′;

RNAi-NRF2: 5′- GGAUGAAGAGACCGGAGAAUUTT-3′.

2.9. Measurements of ROS

To detect the ROS levels in PC12, the cells were stained with dihydroethidium (DHE; CA1420; Solarbio, China) probe which was dissolved in serum-free medium (1:1000 dilution) to a final concentration of 5 μmol/L. Cells were then incubated with DHE for 30 min at 37 °C. The MitoSOX probe (M36008; Thermo Fisher Scientific) was used to detect mitochondria-specific ROS. After dilution at a ratio of 1:1000, it was added to the cell culture medium to assess oxidative stress levels within the mitochondria. MitoTracker Green (C1048, Beyotime Biotechnology, Shanghai, China) was used to label the mitochondria. After being washed with the PBS 3 times, the cells were co-incubated with both MitoTracker Green and MitoSOX for 30 min at 37 °C.

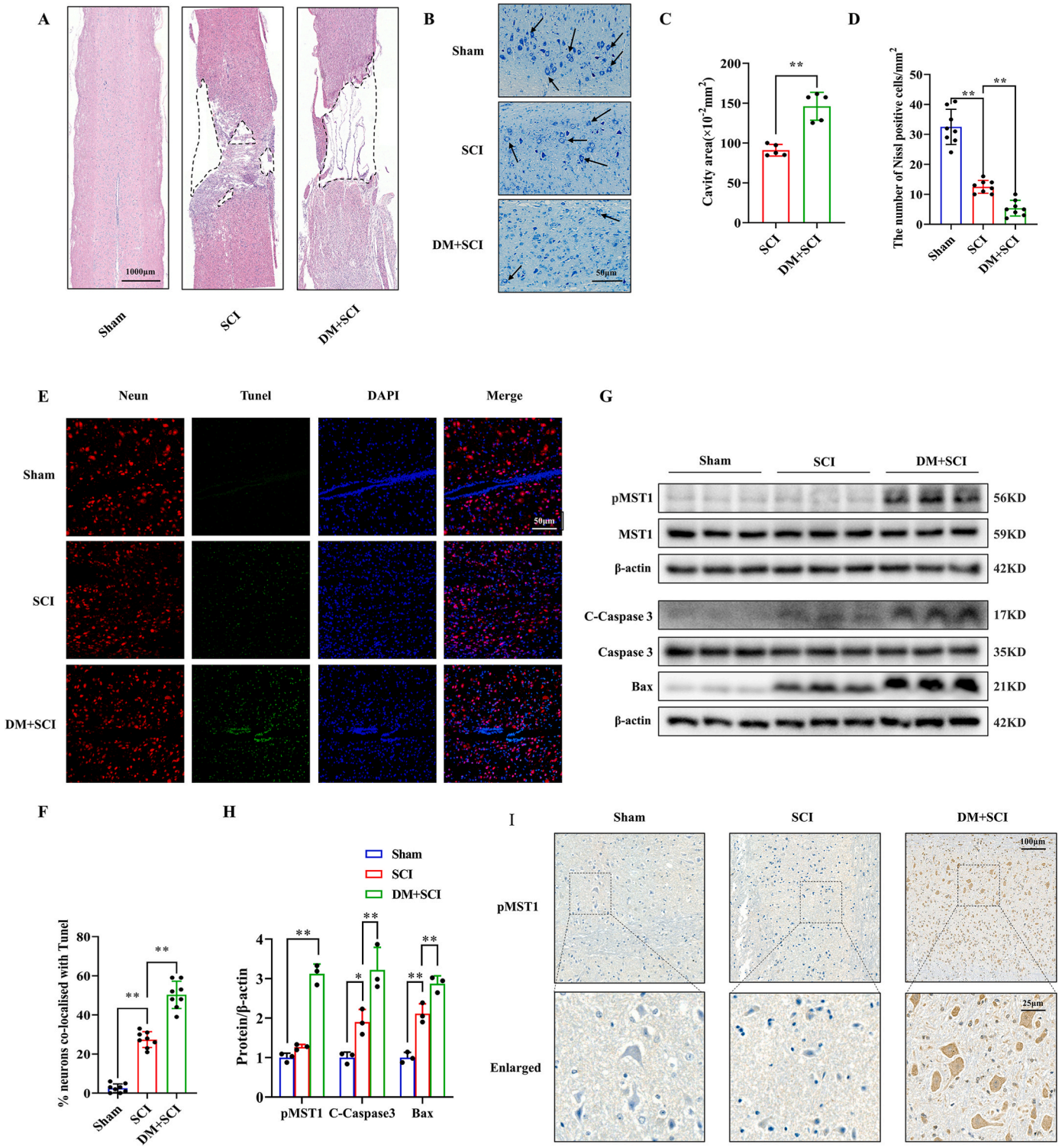

Fig. 1. Histological and protein expression analysis of spinal cord sections from the sham, SCI, and DM + SCI groups. (**A, C**) H&E staining of the spinal cord tissue sections to assess the pathological changes, and the area of cavities for each group is illustrated in a columnar chart. n = 5 mice/group. (**B, D**) Nissl staining was performed to evaluate neuronal survival. Arrows indicate Nissl-positive cells. The column chart illustrates the comparison of Nissl-positive cell numbers among the three groups. n = 8 mice/group. (**E, F**) Double staining for NEUN (red)/TUNEL (green) reveals the proportion of apoptotic (Nissl-positive) cells relative to the NEUN-positive cells. n = 8 mice/group. (**G, H**) Western blots for theMST1, pMST1, Bax, and caspase-3 cleavage, and densitometry analyses are shown. n = 3 mice/group. (**I**) Immunohistochemistry (for pMST1) was used to assess MST1 activation in the three groups. n = 3 mice/group. *P < 0.05 and **P < 0.01.

Fluorescent images were obtained using a fluorescence microscope (400 × magnification; Nikon, Tokyo, Japan).

2.10. Measurements of mitochondrial membrane potential

The mitochondrial membrane potential was measured using a JC-1 staining assay kit (HY-K0601; Mid Columbia Engineering, USA) following the manufacturer's protocol. After intervention, 2 μM of JC-1 was added to the cells and the cells were incubated for 30 min at 37 °C. After washing three times with PBS, images were visualized using a fluorescence microscope.

2.11. Measurements of cell viability

The PC12 cells were prepared in 96-well plates (5×10^3 cells and 100 μL per well) and cultured in a cell incubator for 24 h. Following the respective treatments, 10 μL of CCK-8 (CK04; DOJINDO, Japan) solution was added to each well, and further incubated within the cell culture incubator for 1 h. Finally, the absorbance was measured at 450 nm using a microplate reader (MK3; Thermo Fisher Scientific). Comprehensive information regarding the CCK-8 assay is provided in the Supplementary Material (Fig. S2).

2.12. Apoptosis assay

Annexin V (5 μL) and propidium iodide (PI; 5 μL; BD556547; BD Biosciences, USA) were both added to the cell suspension. After incubation at 37 °C for 10 min, the labeled cells were quantified using a flow cytometry (Beckman Coulter, USA) and at least 10,000 events per sample were recorded.

2.13. Western blot analysis and co-immunoprecipitation

Fresh spinal cord tissues and PC12 cells were lysed using RIPA lysis buffer (Beyotime, China) containing protease and phosphatase inhibitors (Thermo, USA) for 20 min. The protein concentrations were estimated by BCA method (Thermo, USA), and 40 μg of protein extracts were loaded onto an 8% SDS-polyacrylamide gel for electrophoresis and subsequently transferred onto a PVDF membrane (Millipore, USA). The membrane was then blocked with 5% skim milk for 1 h, followed by overnight incubation with primary antibodies at 4 °C. Finally, the cells were thoroughly washed, and incubated with an appropriate HRP-conjugated secondary antibody for 1 h at 37 °C. The primary antibodies against Tuj1, Tomm20, Gap43, HO1, NEUN, NF200, MST1, pMST1, Bax, Bcl2, CytoC, and Caspase 9 were from Abcam (Cambridge, UK), and antibodies against Caspase3, Cleaved Caspase3, Drp1, AKT1 and pGSK3β were from Cell Signaling Technology (USA); *anti*-β-actin, *anti*-β-TrCP, and *anti*-NRF2 were acquired from GeneTex (San Antonio, USA), Santa Cruz Biotechnology (Santa Cruz, CA), and Thermo (Massachusetts, USA), respectively. Those against Cleaved Caspase9, GSK3β, and *p*-AKT1 were from Affinity Bioscience, and those against Ubiquitin, α-tubulin, NOX2, NOX4, SOD2, and NQO1 were purchased from proteintech (Wuhan, China).

For immunoprecipitation, the prepared cells were washed with cold phosphate-buffered saline (PBS) and lysed with RIPA lysis buffer containing protease and phosphatase inhibitors for 20 min. The lysates were incubated with 2 μg desired antibodies overnight at 4 °C along with 20 μL protein A/G-beads. The beads were rinsed seven times with the lysis buffer and boiled in the loading buffer. Subsequent steps were carried out following the procedure described above for western blotting.

2.14. RNA extraction and qPCR

Total RNA was extracted from spinal cord samples using a TRIzol reagent (Thermo Scientific, USA) and from PC12 cells using a total RNA extraction kit (Omega, USA). Subsequently, single-stranded cDNA was synthesized from RNA using PrimeScript RT Master Mix (Takara Bio, Japan). Primers used are listed in Supplementary Table S2. Quantitative PCR was performed using the SYBR Green PCR mix (Takara, Japan) on a LightCycler 480 instrument (Roche, Germany).

2.15. Statistical analysis

The results were presented as means (±SEM) and analyzed using GraphPad Prism software (version 8.3; GraphPad Software Inc., San Diego, CA, USA). The n represented the number of independent experiments or animals per group in each experiment, with its value shown in the figure legend for statistical tests. Normality of data distribution was assessed using the Shapiro-Wilk normality test, and homogeneity of variance was evaluated using the Brown-Forsythe test for multiple groups. Comparisons within groups were made using the unpaired Student's *t*-test between two groups or one-way analysis of variance (ANOVA) for multiple groups. Statistical significance was set at $P < 0.05$.

3. Results

3.1. Neuronal apoptosis and MST1 phosphorylation were increased after SCI in a DM mouse model

Here, we have confirmed the role of diabetes on neuronal apoptosis after SCI. Histological changes were assessed in the three experimental groups (sham, SCI, and DM + SCI) using light microscopy. There was a progressive deterioration in the lesions of the SCI mice when compared to the sham group. For the DM + SCI group, the tissue exhibited larger cavities and greater cellular contraction. The survival of neurons near the lesion site was visualized using Nissl staining of the spinal cord sections that were obtained 28 days after injury. In the SCI group, the Nissl-positive cells were significantly decreased when compared to those in the sham group, while the DM + SCI group showed the lowest number of surviving cells overall (Fig. 1B). Double staining for NEUN (red) and TUNEL (green) was performed to assess neuronal apoptosis around the lesions (Fig. 1E). The proportion of TUNEL-positive cells significantly increased from 2.6% in the Sham group to 28.1% in the SCI group, and 51.9% in the DM + SCI group. The increases were accompanied by increased caspase3 cleavage and Bax expression in the injured spinal cord, and DM further increased the expression of pro-apoptotic proteins.

Given the close association between MST1 signaling, diabetes, and neuronal oxidative damage [20,21], its activity in the spinal cord of the DM and SCI mouse models was determined. Western blot analysis showed that the levels of MST1 phosphorylation (T183) were not significantly different between the sham and SCI mice 14 days after injury, whereas a dramatic increase in pMST1 was observed in the DM + SCI mice when compared to the sham mice (Fig. 1G). MST1 was also activated in the type 2 diabetes mouse model (without SCI) (Figs. S1A–B). To confirm the neuron-specific upregulation of MST1, immunohistochemistry was conducted for pMST1 in the coronal sections of the spinal cord from the three groups of mice. There was distinctive pMST1 staining of the gray matter region neurons of the DM + SCI group, whereas cells from the other two groups exhibited almost no staining (Fig. 1I). Taken together, these results reveal a parallel relationship between neural apoptosis and MST1 activation, suggesting that aggravated neuronal dysfunction in diabetic mice after SCI may be related to the upregulation of MST1.

3.2. AGEs exacerbate oxidative stress and apoptosis in the in vitro SCI model

Spinal cord injuries result in ROS accumulations at the lesion sites, leading to an inevitable oxidative response and neuronal cell death. To further demonstrate the role of DM in exacerbating SCI, TBHP was used as a mediator of oxidative damage. Appropriate drug concentrations

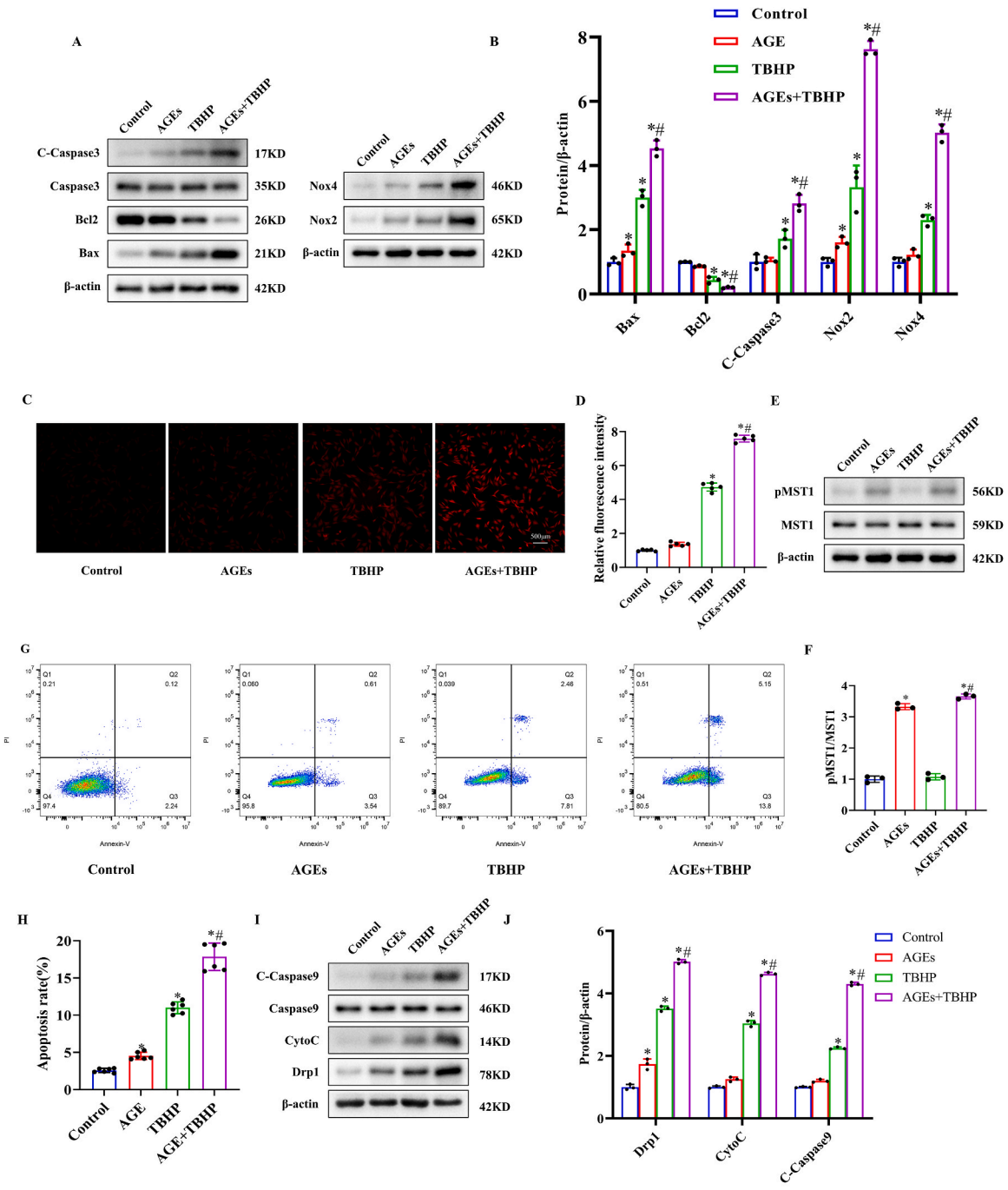

(caption on next page)

Fig. 2. AGEs increase mitochondrial dysfunction and oxidative stress in PC12 cells. (**A** and **B**) Western blot and densitometry analysis of apoptosis-related proteins and the NOX family in the control, AGEs, TBHP, and AGEs + TBHP groups (n = 3 independent experiments for A-B). (**C** and **D**) Representative fluorescence images of DHE (red) staining in cells and quantification of fluorescence intensity (n = 5 independent experiments for *C*-D). (**E** and **F**) Protein levels of MST1 and *p*-MST1 in each group and quantitative analyses are shown (n = 3 independent experiments for *E*-F). (**G** and **H**) Flow cytometry analysis of apoptosis and the proportion of apoptotic cells (n = 6 independent experiments for G-H). (**I** and **J**) Western blot and densitometric analyses of (Cleaved) caspase9, CytoC, and Drp1 (n = 3 independent experiments for I-J). (**K**) Representative fluorescence images with MitoSOX (red) and MitoTracker (green) double staining. (**L**) Representative MMP detected using JC-1 staining (n = 3 independent experiments for K-L). *p < 0.05 compared with the control group and #p < 0.05 compared with the AGEs + TBHP.

were selected to mimic the internal environmental changes in PC12 cells under oxidative and diabetic conditions (Figs. S2A–D). It was shown that the combined treatment with AGEs and TBHP resulted in a more substantial reduction in cellular viability, in contrast to the single application of TBHP. When the PC12 were treated with 25 μg/mL for 24 h, AGE mildly induced proapoptotic Bax protein expression, but this effect was more notable in the TBHP group (10 μM, 6 h). Furthermore, AGEs significantly exacerbated the pro-apoptotic damage induced by TBHP. The NOX family of NADPH oxidases is a crucial enzymatic source of superoxide [33]. The results of immunoblotting and fluorescence intensity measurements indicated that AGEs enhanced the accumulation of superoxide initiated by peroxides, which manifested as an increase in the expression of the NOX family as well as the dihydroethidium (DHE) signal (Fig. 2A–D). The proportion of apoptotic cells in each group was analyzed (Fig. 2G–H) and the AGEs were found result in slight cellular apoptosis (4.15%), which was less pronounced than that observed in the TBHP group (10.27%). However, the most significant increase was observed in the AGEs + TBHP group (18.95%). To elucidate the mechanism underlying the oxidative stress changes caused by AGEs, the activation of MST1 in cells from each group was assessed. As expected, cells treated with AGEs exhibited a greater degree of phosphorylation than the non-AGE groups, while 6-h of TBHP stimulation did not yield such effects.

Apoptosis in neuronal cells is often characterized by the incomplete clearance of ROS and intense destruction of mitochondrial function. ROS disrupts the mitochondrial respiratory chain, causing disturbances in cellular energy metabolism. This, in turn, renders the cell less capable of maintaining redox homeostasis, inevitably resulting in a vicious circle, considering that mitochondria are important organelles involved in the generation of peroxides and the elimination of excess ROS [34]. In this study, we first examined the effects of AGEs and TBHP on mitochondrial function using western blotting. The combination of AGEs and TBHP induced further cleavage of caspase-9 and increased the release of cytochrome *c* and Drp1 when compared with the TBHP treatment alone (Fig. 2I–J). Given that ROS primarily originate from the mitochondria and that decreased mitochondrial membrane potential (MMP) is closely linked to poor mitochondrial function, mitochondrial ROS were detected using MitoSOX assays and MMP with JC-1 staining. There were no obvious fluorescence signal alterations observed between the control and AGEs groups (Fig. 2K-L). However, when subjected to intense oxidative damage by TBHP, the AGEs + TBHP group exhibited increased mitochondrial ROS production when compared with the TBHP group. Furthermore, the fluorescence of the MitoTracker Green decreased with increasing ROS levels, and the red/green fluorescence ratio from the JC-1 staining was much smaller in the AGEs + TBHP group. Taken together, these results indicate that AGEs treatment augmented MST1 activity in the in vitro SCI model. In addition, AGEs promoted the production of cellular ROS, reduced mitochondrial membrane potential, and promoted PC12 apoptosis. It is thus important that the relationship between MST1 and adverse effects induced by AGEs is further investigated.

3.3. Downregulation of MST1 significantly alleviated AGEs-induced neuronal apoptosis and mitochondrial ROS in the in vitro SCI model

To clarify the role of MST1 in AGEs aggravated oxidative injury and mitochondrial dysfunction in SCI, lentiviruses containing shRNA against MST1 (MST1-shRNA) and XMU-MP-1 (MST-1 selective inhibitor) were used to suppress MST1 activity. The knockdown efficiency of MST1 was determined using western blotting. Both MST1 and pMST1expression were notably inhibited by lentivirus transfection, and XMU-MP-1 decreased the phosphorylation of MST1 (Fig. 3A–B). The levels of apoptosis markers, mitochondrial ROS production, and MMP were assessed as previously described. The results showed that knocking down MST1 and inhibiting its phosphorylation significantly enhanced the expression of anti-apoptotic Bcl2 and decreased the expression of pro-apoptotic Bax when compared to the AGEs + TBHP group, implying that MST1 mediated the neuronal damage induced by AGEs (Fig. 3C–D), and these results were consistent with those from the flow cytometry analysis (Fig. 3*E*–F). Furthermore, the percentage of apoptotic PC12 cells drastically increased from 9.3% with the TBHP to 20.63% with the AGEs + TBHP; however, treatment with an MST1 inhibitor and the knockdown of MST1 significantly decreased the proportion (8.16% and 7.33%, respectively). Corresponding changes in mitochondrial homeostasis following the downregulation of MST1 were also detected. It was evident that both XMU-MP-1 and the silencing of MST1 could effectively prevent the increase in mitochondrial pro-apoptotic proteins when compared to the AGE + TBHP group (Fig. 3G–H). This observation was corroborated by the findings of the MitoSOX assays and MMP staining (Fig. 3I–J), which validated that the above-mentioned interventions were able to eliminate excess ROS and maintain a relatively higher membrane potential. In summary, MST1 depletion and chemical inactivation of MST1 suppressed the cellular apoptosis caused by TBHP and AGEs.

3.4. AGEs exacerbated oxidative stress by inhibiting the NRF2-mediated defensive antioxidant response

Previous studies have identified the potential involvement of NRF2-mediated antioxidant transcriptional responses in the pathogenesis of SCI [27,35]. During the early stages of SCI, characterized by severe oxidative stress, the NRF2/ARE system is immediately activated, and this is the primary driver for the transcription of numerous antioxidant enzymes which help to alleviate neuronal death at the epicenter of SCIs [26]. We first analyzed the effect of TBHP on the antioxidant capacity in vitro, and both the mRNA and protein levels of the NRF2 and downstream antioxidant enzymes increased in a time-dependent manner after the PC12 cells were treated with 10 μM TBHP (Fig. S3), indicating that hydrogen peroxide triggered a defense response against excessive ROS.

However, NRF2 has repeatedly been shown to be inhibited in DM models [36,37]. To verify this, NRF2 expression in the injured spinal cord was determined by western blotting 14 d after the SCI (Fig. 4A). The results showed that the level of NRF2 increased when compared to that in the sham group, while the SCI-induced antioxidant responses were suppressed by DM. To explore the underlying mechanisms, the transcriptional differences in antioxidant-related genes in the PC12 cells exposed or unexposed to AGEs were examined (Fig. 4C). Interestingly, the mRNA level of the NRF2 was enhanced, while the expression of downstream genes such as NQO-1, Catalase, HO-1, and SOD2 were all significantly decreased. Subsequently, we performed immunoblotting and densitometric analysis (Fig. 4D–E) for NRF2, NQO-1, HO-1, and SOD2 in PC12 cells from the control, AGEs, TBHP, and AGEs + TBHP groups. The application of AGEs for 24 h was found to decrease antioxidant enzyme expression. It was thus hypothesized that NRF2 might not be hindered at the transcriptional level but at the post-transcriptional level. Conversely, these proteins were amplified

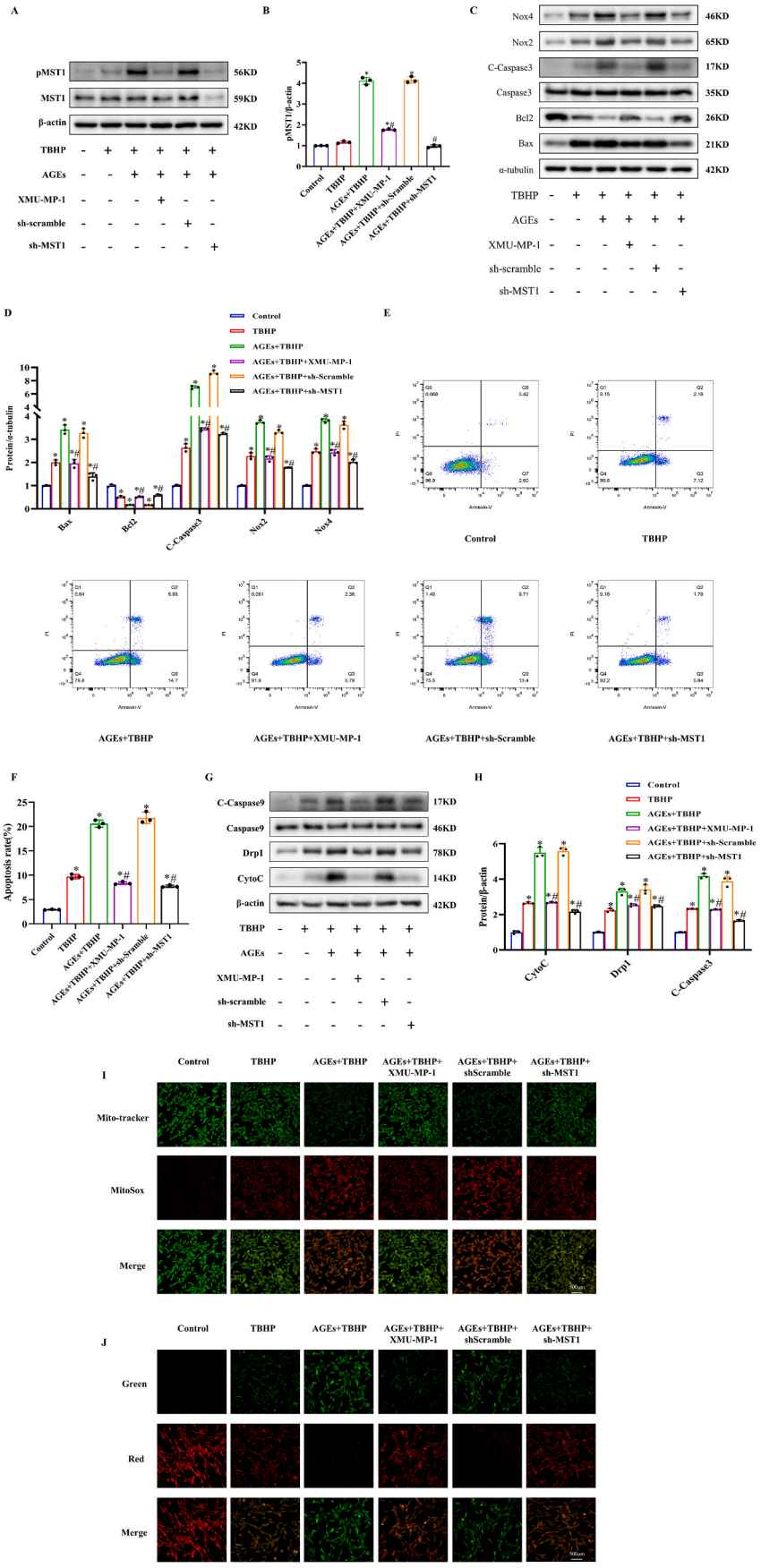

(caption on next page)

Fig. 3. Downregulation of MST1 attenuates AGEs aggravated mitochondrial dysfunction and apoptosis in vitro. (**A** and **B**) Western blot and densitometric analysis of MST1 and *p*-MST1 in six cell lines (n = 3 independent experiments for A-B). (**C** and **D**) Western blot and densitometric analysis of apoptosis-related proteins and the NOX family in the six groups (n = 3 independent experiments for *C*-D). (**E** and **F**) Analysis of apoptotic ratio in injured cells with or without MST1 inhibition (n = 3 independent experiments for *E*-F). (**G** and **H**) Western blotting and densitometry analyses of CytoC, Drp1, and Caspase9 cleavage (n = 3 independent experiments for G-H). (**K**) Representative fluorescence images with MitoSOX (red) and MitoTracker (green) double staining. (**L**) Representative MMP detected using JC-1 staining (n = 3 independent experiments for K-L). *p < 0.05 compared with the control group and #p < 0.05 compared with the AGEs + TBHP.

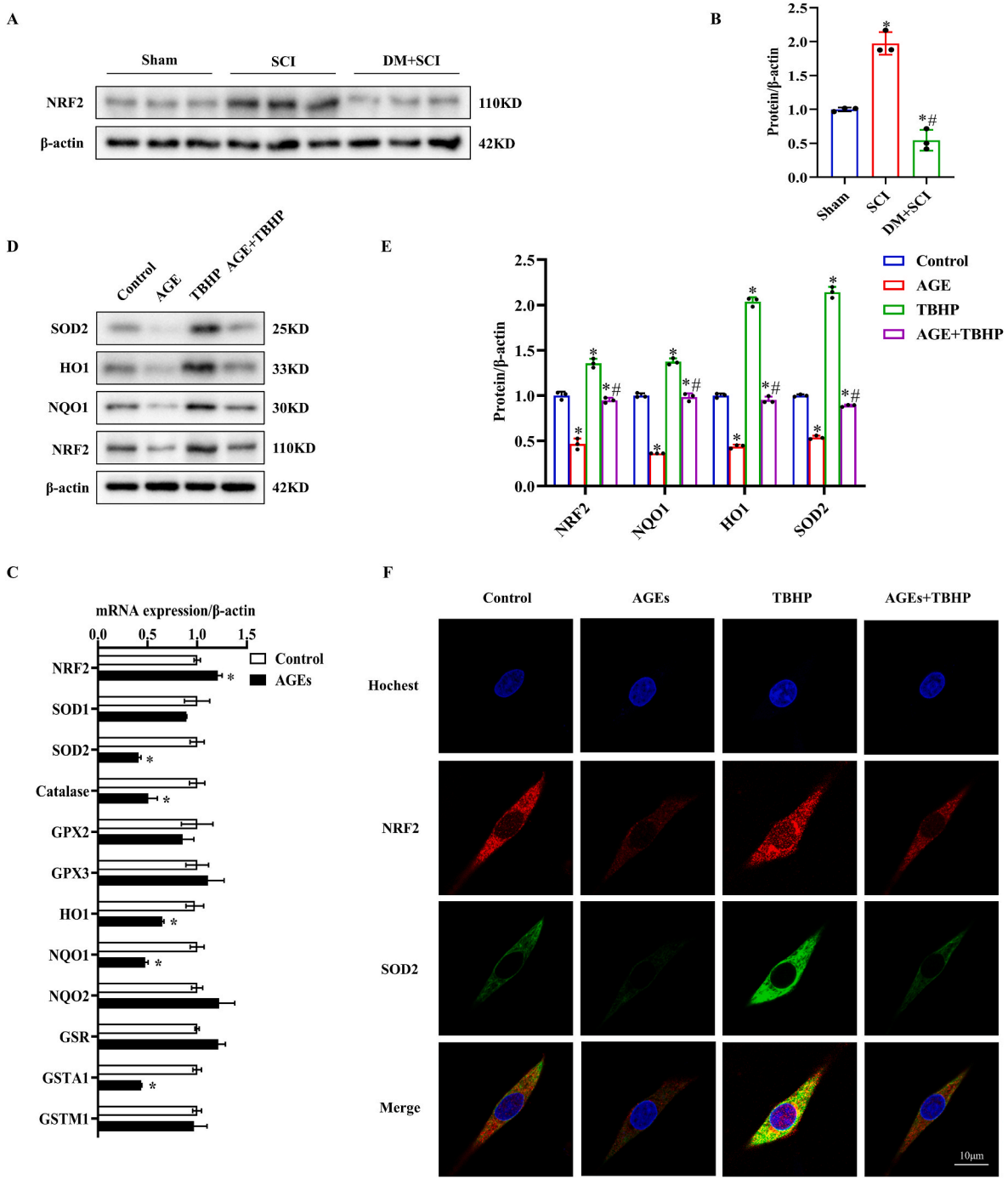

Fig. 4. Neuoronal antioxidant capacity was diminished in vivo and in vitro with the diabetes SCI model. (**A** and **B**) Representative immunoblot analyses of the Sham, SCI, and DM + SCI spinal cord samples (n = 3 independent experiments for A-B). (**C**) The mRNA levels of NRF2, NQO1, HO1, and SOD2 in control and AGEs PC12 cells (n = 3 independent experiments for C). (**D** and **E**) Western blot and densitometric analysis of antioxidant elements in cells from the control, AGEs, TBHP, and AGEs + TBHP groups (n = 3 independent experiments for D-E). (**F**) Representative fluorescence images of NRF2 (red) and SOD2 (green) double-staining in PC12 cells (n = 3 independent experiments for F). *p < 0.05 compared with the control and #p < 0.05 compared with the AGEs + TBHP.

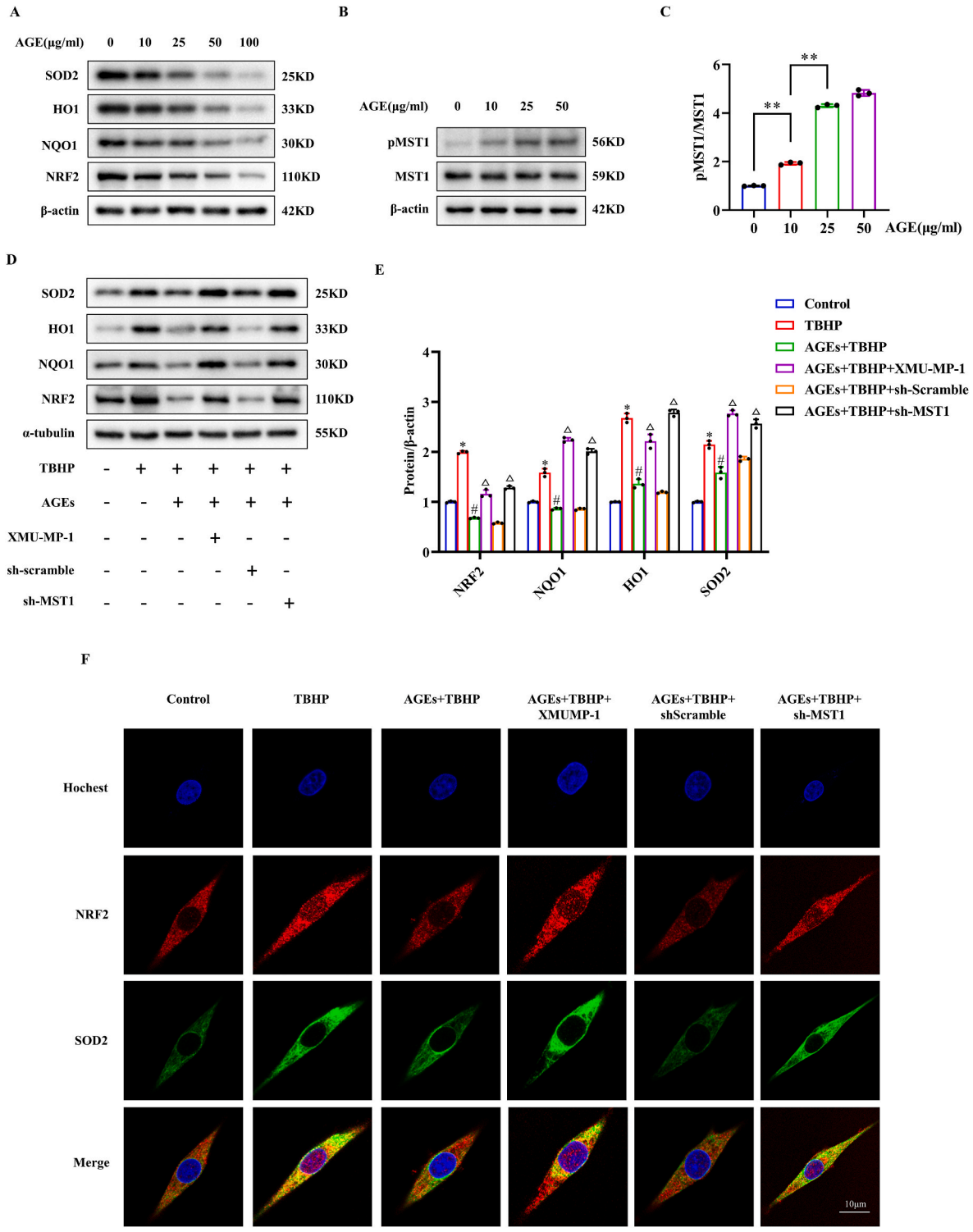

Fig. 5. MST1 inhibition improved the antioxidant capacity suppressed by AGEs in PC12. (**A**) NRF2, NQO1, HO1, and SOD2 expression levels in PC12 cells treated with different AGEs concentrations for 24 h were evaluated using a Western blot analysis. (**B** and **C**) Representative immunoblot bands for *p*-MST1 (T 183), MST1 in PC12 cells treated with different AGEs concentrations for 24 h (n = 3 independent experiments for A-C). (**D** and **E**) Western blot and densitometric analysis of antioxidant elements in cells from each group (n = 3 independent experiments for D-E). (**F**) Representative fluorescence images of NRF2 (red) and SOD2 (green) double-staining in PC12 cells (n = 3 independent experiments for F). *p < 0.05 compared with the control, #p < 0.05 compared with the TBHP, and △ p < 0.05 compared with the AGEs + TBHP.

when PC12 cells were treated with TBHP for 6 h, but this increase interfered with the supplementary AGEs. These results were consistent with immunofluorescence staining, as this showed that the expression of NRF2(Red) and SOD2(Green) in the TBHP group was higher than that in the control group, and augmented NRF2 nuclear accumulation was also observed, while their expression was lower in the AGEs + TBHP group (Fig. 4F). Collectively, these results suggest that DM inhibits the antioxidant system activated by sudden oxidative stress.

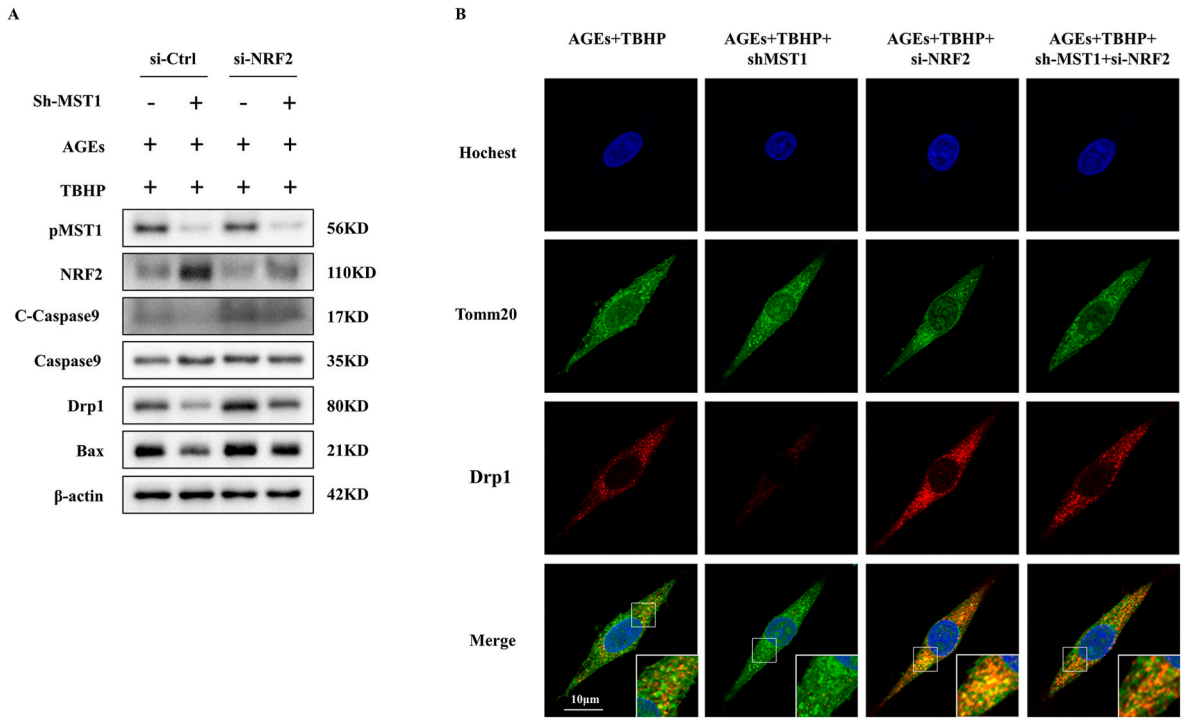

Fig. 6. NRF2 knock-down abolishes the protective effect of MST1 inhibition against mitochondrial dysfunction and apoptosis. (A) Western blot and densitometric analysis of (Cleaved) Caspase9, Drp1, and Bax in the AGEs + TBHP, AGEs + TBHP + shMST1, AGEs + TBHP + si-NRF2, and AGEs + TBHP + sh-MST1+si-NRF2 groups. (**B**) Representative fluorescence images of Tomm20 (green) and Drp1 (red) double-staining in PC12 cells (n = 3 independent experiments for A-B).

3.5. Downregulation of MST1 confers antioxidant protection by activating NRF2

Previous studies have reported that the kinase MST1 modulates the cellular redox balance via the stability of the antioxidant transcription factor NRF2 [29,38]; however, the relationship between MST1 and NRF2 in the nervous system is not yet fully understood. This study thus investigated whether the downregulation of MST1 ameliorated neuronal oxidative damage through the NRF2 pathway. Immunoblotting measurements of PC12 lysates revealed that NRF2, HO1, SOD2, and NQO1 expression levels were all significantly reduced by AGE supplementation, whereas both XMU-MMP-1 and lentivirus containing shMST1 significantly reversed these changes (Fig. 5D). In other words, antioxidant enzymes were restored, and NQO1 and SOD2 surpassed the levels observed in cells treated with TBHP, providing effective cellular protection. NRF2 is a core transcription factor primarily active within the nucleus, and the immunofluorescence analysis showed that it exhibits remarkably higher nuclear translocation in MST1-inhibited cells when compared with the AGEs + TBHP-treated cells (Fig. 5F). Furthermore, there was significant enhancement in the fluorescence intensity of downstream SOD2 which is located on the mitochondrial inner membrane, thereby struggling to maintain mitochondrial function. Overall, these results suggest that MST1 inhibition improves the cellular antioxidant capacity suppressed by AGEs.

3.6. Silencing NRF2 reversed the protective effect of MST1 inhibition on apoptosis via a mitochondrial-dependent pathway

To further confirm that NRF2 plays a causative role in mitigating mitochondrial apoptosis, NRF2 was knocked down with siRNA in TBHP + AGEs cells that were or were not pretreated with shMST. Indeed, compared to the AGEs + TBHP and AGEs + TBHP + shMST1 groups, the reduction in NRF2 triggered greater cleavage of caspase-9 and increased Drp1 and Bax (Fig. 6A). The knockdown of NRF2 rendered the antioxidant system less capable of defending against oxidative stress, overshadowing the rescue effect of the sh-MST1 on mitochondrial function. Dual-label staining for the mitochondrial fission protein Drp1 and Mitochondrial 20 kDa outer membrane protein (Tomm20) was then conducted. Knocking down MST1 resulted in the Drp1 being less dispersed without any specific localization within the mitochondria. However, in the NRF2 knockdown group, it exhibited significant co-localization with Tomm20 (Fig. 6B). The results indicate that the MST1 inhibition likely exerts its protective effect against AGE-exacerbated mitochondrial dysfunction by restoring NRF2 levels.

3.7. MST1 downregulation attenuated the ubiquitination of NRF2 via AKT1/GSK3β/β-TrCP axis

As a result of the notable decrease in the transcription of genes encoding antioxidant enzymes in AGE-treated PC12 cells and the crucial role of NRF2 in the MST1 knockdown, the mechanism by which MST1 modulates NRF2 expression was explored. Non-significant changes were found in the mRNA levels of NRF2 using the in vivo diabetic model (Fig. 7A); however, NRF2 and SOD2 protein levels were significantly reduced in DM mice when compared to those in the control, suggesting that diabetic conditions might interfere with NRF2 protein stability (Fig. 7B and S4). NRF2 is primarily degraded via the ubiquitin-mediated proteasomal pathway. In essence, the stabilization and nuclear localization of NRF2 are regulated by Keap1 and β-TrCP, which are two E3 ubiquitin ligase adaptors [39]. To investigate the molecular mechanisms of MST1 and NRF2, the predicted target genes including NFE2L2 and STK4, were uploaded into the STRING and GeneMANIA databases to create protein-protein interaction networks. Both studies suggested that MST1 can interact with NRF2 via these two E3 ubiquitin ligases, influencing protein stability and apoptosis mediated by oxidative stress. Under non-stress conditions, the NRF2 protein within the cell is maintained at very low levels because of its inhibitor, Keap1 [40]. In immune cells, MST1/2 disrupts the dimerization and polymerization of Keap1, thereby blocking the ubiquitination and degradation of NRF2 and protecting cells from oxidative stress-induced aging [38]. Nonetheless,

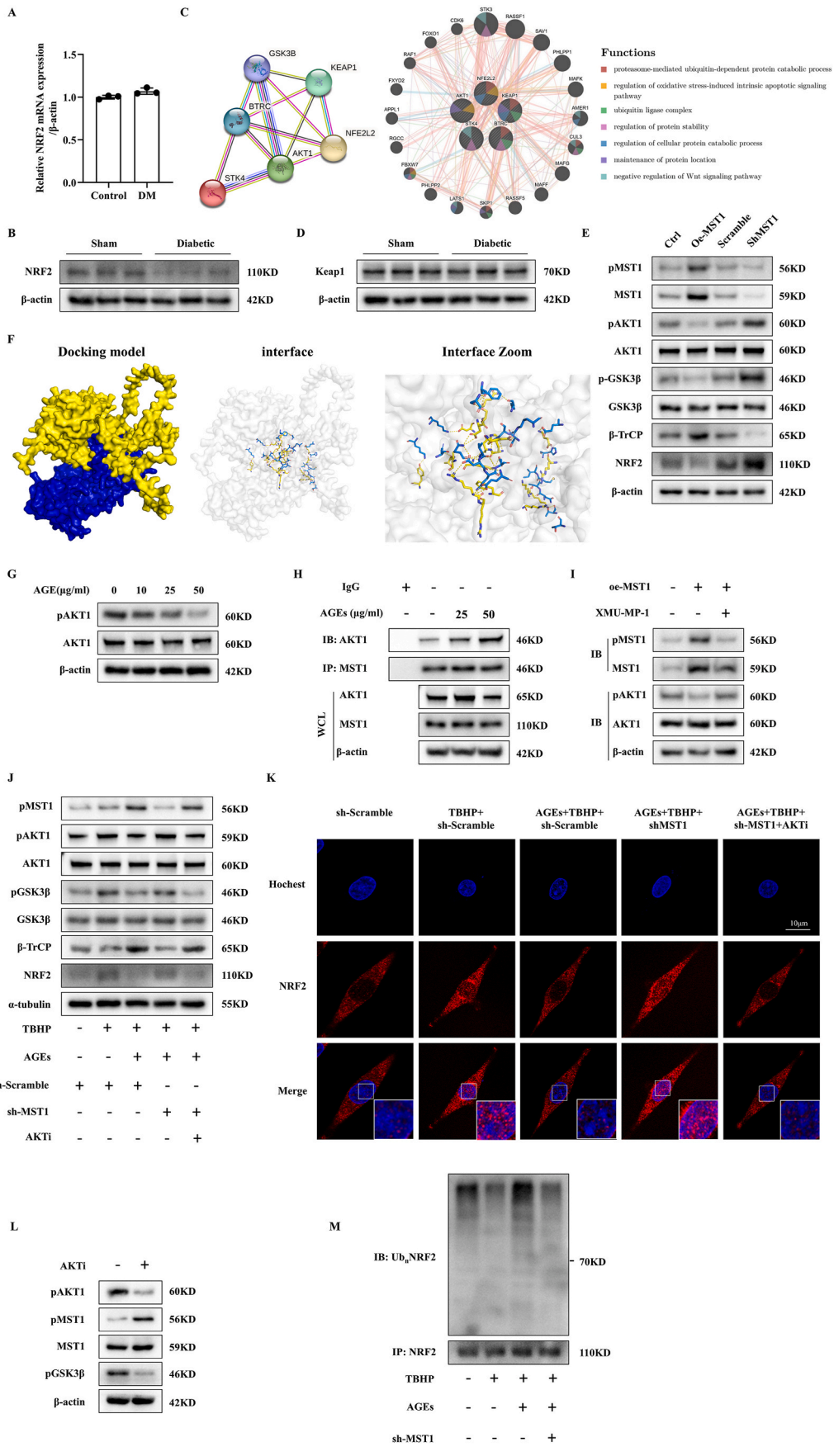

(caption on next page)

Fig. 7. MST1 knockdown decreases ubiquitination of NRF2 via AKT1/GSK3β/β-TrCP axis. (A) RT-qPCR analysis of the NRF2 mRNA levels in vivo (n = 3 independent experiments for A). (**B**) Western blot analysis of NRF2 in the spinal cord lysates of control and diabetic mice. (**C**) PPI network analysis revealed a relationship between MST1 and NRF2. The graph on the left shows the STRING analysis, and that on the right shows the GeneMANIA analysis. (**D**) Western blot analysis of Keap1. (**E**) Western blot analysis of MST1, AKT1, GSK3β phosphorylation, β-TrCP, and NRF2 (n = 3 independent experiments for B, D and E). (**F**) Surface diagram of the docking model and the interfacing residues between MST1 and AKT1 (MST1, yellow; AKT1, blue; hydrogen bond interaction, dotted line). (**G**) Phosphorylation in AKT1 with different concentrations of AGEs in the PC12 cells. (**H**) Immunoprecipitation analysis of the interactions between MST1 and AKT1. (**I**) Western blot analysis of AKT1 phosphorylation in PC12 cells treated with lentiviral vectors overexpressing MST1 or XMU-MP-1. (**J**) Western blot analysis of pMST1, *p*-GSK3β/total GSK3β, and *p*-AKT1/total AKT1 in vitro. (**K**) Representative fluorescence images of NRF2 (Red) in PC12 cells (n = 3 independent experiments for G-K). (**L**) Western blots of pMST1, pAKT1, and pGSK3β from PC12 cells exposed to the AKT inhibitor triciribine (AKTi, 10 μM for 6 h). (**M**) Immunoblot showing the ubiquitination of NRF2 in treated cells (n = 3 independent experiments for L-M).

immunoblotting showed that there were no significant changes in Keap1 expression between the spinal cords of hyperglycaemic mice and controls, indicating that MST1 activation affects NRF2 stability in a Keap1-independent manner in the DM model.

Moreover, evidence suggested that β-TrCP forms a complex with Cullin-1 to create a complete E3 ligase, which facilitates the glycogen synthase kinase 3 (GSK3)-dependent degradation of NRF2 in liver inflammation or nephropathy [41,42]. Although the mechanism responsible for this phenomenon, especially in the nervous system, remains unclear, and consequently, the effects of MST1 over-expression and deletion in PC12 cells were investigated. These results indicate that over-expressing MST1 activates β-TrCP and this results in the downregulation of pAKT1 and pGSK3β(Ser 9). Conversely, β-TrCP levels were lower in the MST1-depleted PC12 cells. The phosphatidylinositol 3-kinase (PI3K)/AKT pathway is a key pro-survival cellular pathway in various disease models [43]. AKT1 reduces the levels of oxygen free radicals and protects cells against toxins and cell death, and GSK3β is a characteristic substrate [43]. Gradually increasing concentrations of AGEs reduced AKT1 phosphorylation (Fig. 7G). It was previously reported that MST1 and its caspase cleavage products can directly antagonize AKT1 activity in mammalian cells [44]. It was thus hypothesized that MST1 is directly linked to AKT1 in diabetic animals. To confirm this association, a rigorous protein-protein docking analysis of MST1 and AKT1 was conducted. MST1 and AKT1 formed hydrogen bonds at specific amino acid residue locations including GLU 149-GLU 461, and LYS 183-ASP 315 (Fig. 7F and Table S3). This observation indicated the formation of a robust protein docking model between MST1 and AKT1. Furthermore, the co-IP experiment confirmed that the products of glycemic metabolism, AGEs, markedly affected pAKT1/AKT1 (Fig. 7H), while treatment with XMU-MP-1 could reverse this inhibitory effect on AKT1 (Fig. 7I). It was subsequently confirmed that 6-h of TBHP stimulation and the knockdown of MST1 could enhance the phosphorylation of AKT1 and the stability of NRF2, while being exposed to the AGEs (25 μg/mL for 24 h) or AKT inhibitor triciribine (AKTi, 10 μM for 6 h) had the opposite effect (Fig. 7J). Immunofluorescence assays also showed that the knockdown of MST1 increased the fluorescence intensity and nuclear accumulation of NRF2 (red), suggesting that MST1 mediates NRF2 degradation and nuclear exclusion via AKT1 inactivation (Fig. 7K). Interestingly, MST1 signaling was moderately upregulated by AKT1 inhibition (Fig. 7L), and it was thus speculated that this might enhance MST1 activation. Furthermore, there may have been some degree of activation of the MST1 in response to the oxidative damage, but compensatory AKT1 phosphorylation suppressed this change. Finally, co-immunoprecipitation and immunoblot assays showed that the polyubiquitination of NRF2 was significantly enhanced in the AGEs + TBHP group when compared to the TBHP group, whereas the knockdown of MST1 decreased the ubiquitination levels of NRF2. Additionally, NRF2 was ubiquitinated and degraded in the absence of stress (Fig. 7M). Taken together, these results reveal that the MST1 knockdown was involved in NRF2 nuclear accumulation and stabilization via the AKT1/GSK3β (Ser9)/β-TrCP pathway.

3.8. AAV-siMST1 increased NRF2-mediated antioxidant activity in vivo and promoted the functional recovery of diabetic mice with SCI

To further determine whether MST1 inhibition could enhance the stability of NRF2 in stressed neurons, adenoviruses carrying siMST1 were injected into the spinal cord of mice with the onset of SCI, and the in vivo experimental design is shown in Fig. 8A. Blood glucose concentrations and body weights were measured before and 2 weeks after STZ injection, and alterations in naïve and STZ-treated mice are summarised in Fig. 8B–C. The blood glucose concentrations in the diabetic mice were significantly elevated, with a decrease in body weight prior to surgery, when compared to the control group. On the 7th day post-SCI, there was abundant NRF2 staining in neurons within the spinal cords of both SCI-operated and DM + SCI + AAV-siMST1 animals compared with the sham mice (Fig. 8D–E). Conversely, following the induction of hyperglycaemia, the fluorescence intensity of NRF2 was much lower in the DM + SCI and AAV vehicle-treated groups. Furthermore, a moderate increase in NRF2 signaling was observed in all mice, except for the sham group, 2 weeks after surgery. This may be due to the limited adaptive ability of the antioxidant enzymes, as a mild reduction in positive signals was observed at 4 weeks post-SCI, but the fluorescence of neurons infected with AAV-siMST1 remained at the highest level. Given that the subacute phase (48 h–2 weeks) is the peak period for the generation of ROS and RNS following SCI [3]. HO1 levels were examined on day 14, and the changes were similar to those of NRF2. Furthermore, the administration of AAV-siMST1 increased the expression of HO1. Although diabetes induced excessive oxidative stress, preventing the negative regulation of MST1 toward NRF2 increased the activity of catalase and GSH, thereby inhibiting the production of the oxidative product, MDA (Fig. 8J-L).

To verify the therapeutic effects of the MST1 knockdown in vivo, a series of experiments were conducted to assess both histological and functional recovery. Initially, we assessed protein expression related to mitochondrial dysfunction and apoptosis, such as cleaved caspase-9 and Bax, 14 days post-SCI (Fig. 9A). The cleaved Caspase-9 and Bax expression levels were both suppressed in the mice from the DM + SCI + AAV-siMST1 group, whereas the presence of DM exacerbated the outcomes of SCI. Administration of AAV-siMST1 prevented the SCI outcomes from worsening in the STZ-induced hyperglycaemic mice. These findings were consistent with the results of haematoxylin and eosin (H&E) staining, where the DM + SCI group exhibited a larger lesion volume than the sham and SCI-only groups. Furthermore, DM + SCI + AAV-siMST1 mice displayed a smaller lesion volume and a more intact tissue structure than the DM + SCI and DM + SCI + AAV-vehicle groups (Fig. 9B–C). Nissl staining and immunofluorescence were used to analyze the therapeutic effects. Both Nissl staining and dual staining for the neuronal cytoskeletal protein neurofilament 200 (NF200, Green) and NEUN (red) revealed that AAV-siMST1 better preserved the integrity of neural tissue when compared to the DM + SCI group and even showed superior therapeutic outcomes in terms of neuronal preservation when compared to the SCI-only mice (Fig. 9D–F). Western blot assays of neuronal structural and synaptic components confirmed the corresponding changes in these groups. Moreover, the performance of the DM + SCI and DM + SCI + AAV-vehicle groups was worse than that of the SCI mice according to the BMS score (Fig. 8H), incline angle test

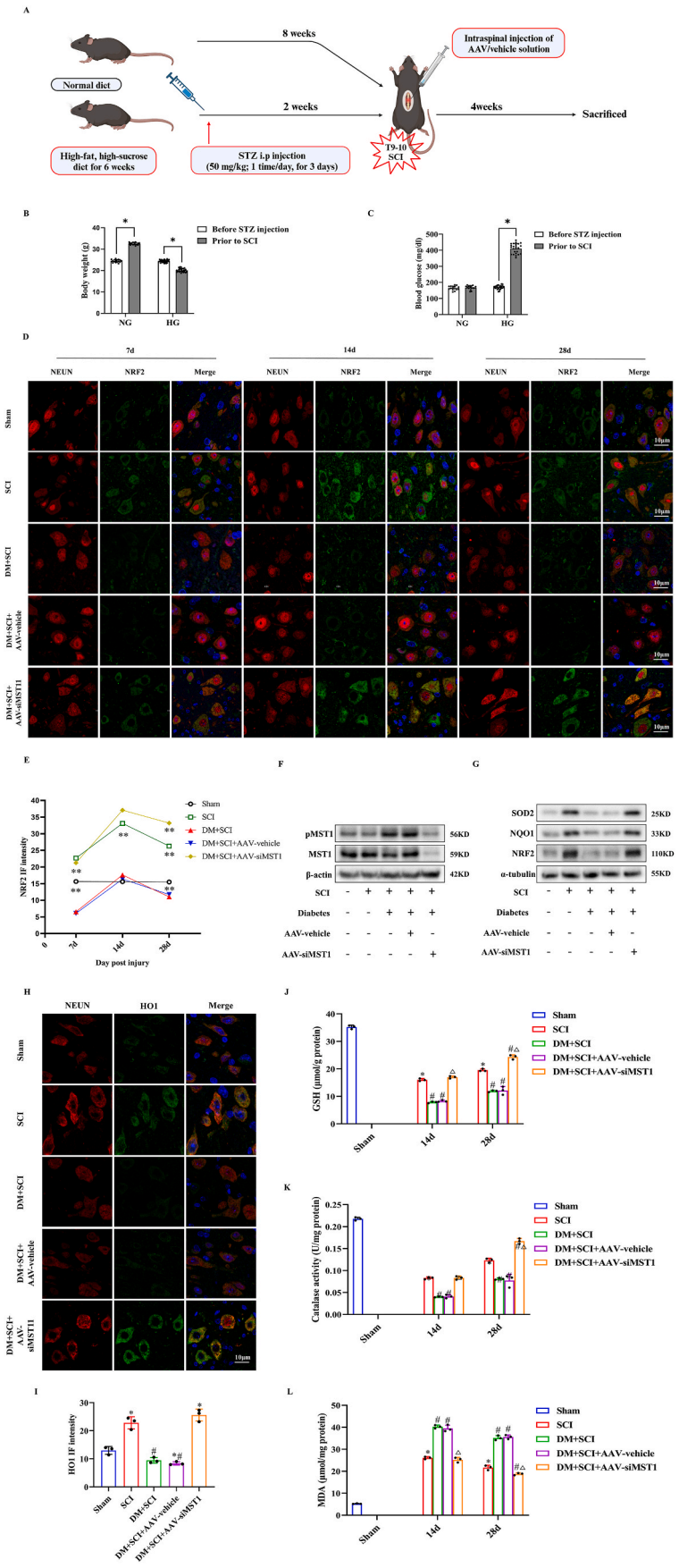

(caption on next page)

Fig. 8. MST1 knockdown increased neuronal NRF2-mediated antioxidant activity in vivo. (**A**) Schematic showing the experimental design involving the animal. (**B** and **C**) Blood glucose concentrations and body weights of naïve and diabetic mice before and two weeks after STZ injection. n = 3 mice/group. (**D** and **E**) Immunofluorescence assay of spinal cord sections under different conditions 7, 14, and 28 days after the operation and quantification of staining fluorescence intensity for NRF2. (**F** and **G**) Western blot analysis for MST1, pMST1, NRF2, NQO1, and SOD2. n = 3 mice/group. (**H** and **I**) Representative fluorescence images of NEUN (red) and HO1(Green) in neurons 14 days after surgery. n = 3 mice/group. Quantification of GSH (**J**), catalase (**K**), and MDA (**L**) in the spinal cord 14 and 28 days after sci administration. *p < 0.05 compared with the Sham group. n = 3 mice/group. #p < 0.05 compared with the SCI group. △ p < 0.05 compared with the DM + SCI group.

(Fig. 8I), and footprint analysis (Fig. 8J), and the MST1-knockdown mice exhibited greater functional outcomes than the SCI-only group 21 days after injury. Taken together, these data indicate that the MST1 deletion increases NRF2-mediated antioxidant capacity in neurons and reduces neuronal apoptosis in diabetic animals after SCI (see Fig. 10).

4. Discussion

Spinal cord injury (SCI) causes devastating damage to the motor and sensory functions of patients. Furthermore, for patients with preexisting diabetes, which is a prevalent metabolic disorder, the difficulties experienced during the functional recovery from a SCI are even greater [4,11]. However, the underlying mechanism by which diabetes mellitus aggravates SCI is unclear. This study has aimed to address this and produced several key findings. First, is that in a SCI animal model, diabetes was found to induce excessive activation of MST1, which further impaired motor function and neuronal apoptosis. While an MST1 knockdown was found to alleviate mitochondrial dysfunction and reduce oxidative damage. Second, in cultured PC12 cells and a spinal cord mouse model, MST1 silencing facilitated the NRF2-mediated antioxidant defense system against oxidative stress after SCI. Third, is that the protective effect against diabetes-aggravated SCI was mediated by the GSK3β/β-TrCP/NRF2 pathway. Collectively, this study has revealed that MST1 inhibition may be a key target for the treatment of diabetes when combined with SCI.

Neurons, the fundamental units of the nervous system, are rich in mitochondria and rely heavily on mitochondrial ATP production for growth, function, and regeneration. Mitochondria serve as ATP factories and are the main sources of free radicals. However, the overproduction of free radicals is detrimental to normal mitochondrial function. Recent experimental studies have shown that the spinal cord exhibits high mitochondrial oxidative metabolism and is extremely sensitive to hypoxic injury [45–47]. It is thus vital that a dynamic balance is maintained in terms of cellular oxygen content to facilitate neuronal energy metabolism in patients with SCI. The increasing prevalence of diabetes has subsequently resulted in an increased incidence of emergency trauma cases, especially in relation to SCI, which is accompanied by hyperglycaemia [9]. Oxidative stress is a key factor in diabetes-related complications, and consequently, the oxidative level changes in patients with DM after SCI are monitored and considered. The impact of diabetes on the neural system has been extensively studied, however, most studies have focused on the association between long-term hyperglycaemia and chronic neurodegenerative diseases [6]. Consequently, our understanding of the effects of diabetes on acute traumatic nervous system injuries is limited. Exploring the role of glucose metabolism disorders in exacerbating SCI and seeking effective treatment methods are both critical issues in this field. This work has shown that diabetes affects acute neural injury by increasing ROS and disrupting mitochondrial functioning, and that the microenvironment of the diabetic spinal cord also accumulates increasing levels ROS derivatives, such as MDA.

MST1 promotes cell death, and a study has reported that a high-fat diet and treatment with palmitic acid induced activation of the MST1/JNK/Caspase-3 (Casp-3) signaling pathway, resulting in neuronal cell apoptosis [48]. Additionally, decreased MST1 phosphorylation protects the brain from neurobehavioral impairments following intracerebral haemorrhage [19]. Surprisingly, in the present study, neither the spinal cord tissue 14 days post-injury nor the PC12 cells under short-term oxidative stress exhibited significant MST1 activation, whereas AKT1 phosphorylation was increased (Fig. 7J). AKT1 is the most prevalent AKT subtype. Several studies have indicated a potential negative feedback mechanism that links MST1 to *p*-AKT. MST1 and its cleaved form act as direct AKT1 inhibitors [44]. On one hand, activated AKT could suppress the activity of MST1 [43]. Consistent with these results, our data also showed that as MST1 (T183) phosphorylation increased, the direct inhibition of *p*-AKT1 became stronger. Conversely, AKT1 inhibition in triciribine-treated cells increased MST1 activity. Taken together, the results indicate that during the subacute phase, the pro-survival PI3K/AKT1 pathway serves as a crucial suppressor of MST1, thus preventing its activation.

The PI3K/AKT pathway is critical for the regulation of the expression of cytoprotective genes, particularly those involved in antioxidant defense [49]. In a cellular model of oxidative stress-induced cell death, short-term exposure to hydrogen peroxide triggered AKT activation [50]. Additionally, a range of NRF2-regulated antioxidant enzymes was increased in the SCI model in vitro, whereas treatment with triciribine, a specific AKT inhibitor, suppressed NRF2 expression. This strongly suggests that the activation of the PI3K/AKT axis is the molecular basis of the neuroprotective effect. NRF2 regulates genes possessing a common *cis*-acting enhancer known as the antioxidant response element (ARE), and this has been suggested to be a central coordinator in protecting against oxidative and inflammatory threats. Numerous reports have confirmed that an increase in the levels of antioxidant enzymes, including SOD2 and HO1, is common during the initial phases of disease progression. Notably, the NRF2/ARE system is immediately activated after SCI to maintain redox homeostasis [26]. This phenomenon may be linked to the early compensatory mobilization of antioxidant capabilities via the PI3K/AKT pathway. The results of this study have also revealed that, in neurons 14 days after SCI, the amount of NRF2 protein was increased when compared to the sham group. In TBHP-treated PC12 cells, both NRF2 and its associated antioxidant components showed time-dependent increases in mRNA and protein levels. However, the experiments showed that diabetes impaired NRF2 antioxidant defense, leading to reduced NRF2 nuclear accumulation and weakened downstream target antioxidant enzymes in both the SCI animal model and PC12 cells. In patients with diabetes and in animals, various vital organs, such as the heart [51], pancreas [43], and brain [48], may trigger MST1 phosphorylation. Diabetes alone has little impact on locomotor function [52]; however, concurrent metabolic disorders can negatively affect the PI3K/AKT signaling pathway, which is activated to rescue surviving neurons. This highlights the importance of paying clinical attention to metabolic regulation in spinal cord injury patients with SCI.

Next, we examined pMST1 expression in spinal cord injury tissues with DM and found that it was increased in neurons. Moreover, diabetes was found to attenuate antioxidant defenses both in vivo and in vitro. Subsequent experiments revealed that AAV-siMST1 in mice at the onset of SCI augmented the expression of NRF2, NQO1, HO1, SOD2, catalase, and GSH, which was suppressed by diabetes, indicating that MST1 may act upstream of NRF2. Further studies are required to fully elucidate the signaling mechanisms of AKT1-NRF2. These changes significantly improved locomotor function and reduced neuronal apoptosis in mice. Previous reports have suggested that NRF2 regulates the expression of several key components of mitochondrial biogenesis, mitophagy, autophagy, and mitochondrial function in the peripheral and central nervous systems [53]. In this study, the fluorescent staining of live cells showed

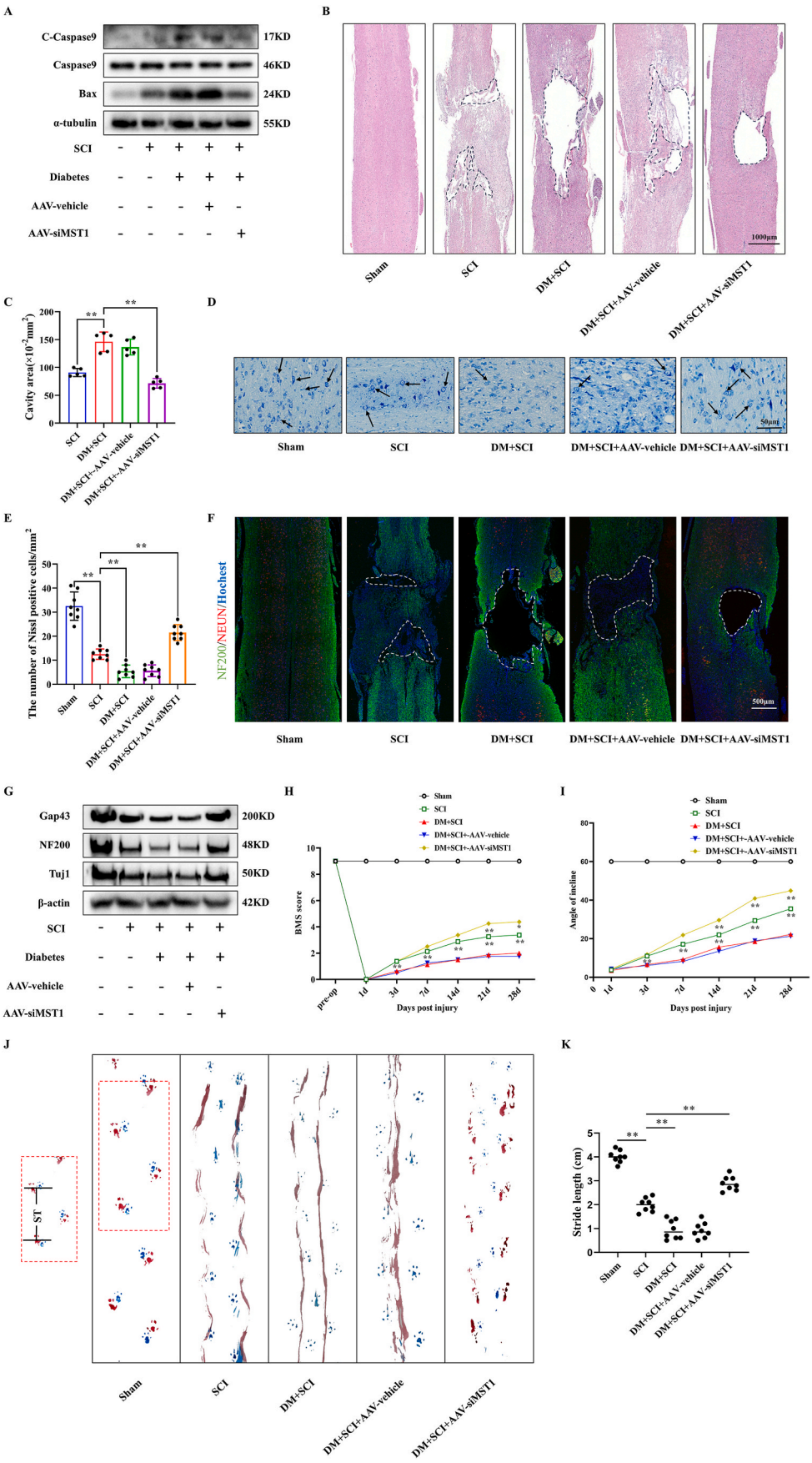

(caption on next page)

Fig. 9. MST1 deletion reduces neuron apoptosis in diabetic mice after SCI. (**A**) Western blot analysis of Bax and Caspase9 cleavage. n = 3 mice/group. (**B** and **C**) Representative images and cavity area quantification of lesion size (H&E staining) in the five groups of mice 28 days post injury. n = 5 mice/group. (**D** and **E**) Nissl staining was performed to evaluate neuronal survival. Arrows indicate Nissl-positive cells. The column chart illustrates the comparison of Nissl-positive cell numbers among the five groups. n = 8 mice/group. (**F**) Representative immunostaining images of NF200 (green) and NEUN (red) in the spinal cord tissues from each group. n = 3 mice/group. (**G**) Western blot analysis of Tuj1, NF200, and Gap43. n = 3 mice/group. (**H** and **I**) BMS and inclined plane test scores of mice 1, 3, 7, 14, 21, and 28 days after surgery. n = 8 mice/group. (**J** and **K**) Footprint analysis was performed 28 days after injury. The front limbs are marked with blue dye, and the rear limbs are marked with red dye. Stride length was measured. n = 8 mice/group. *p < 0.05 and **p < 0.01.

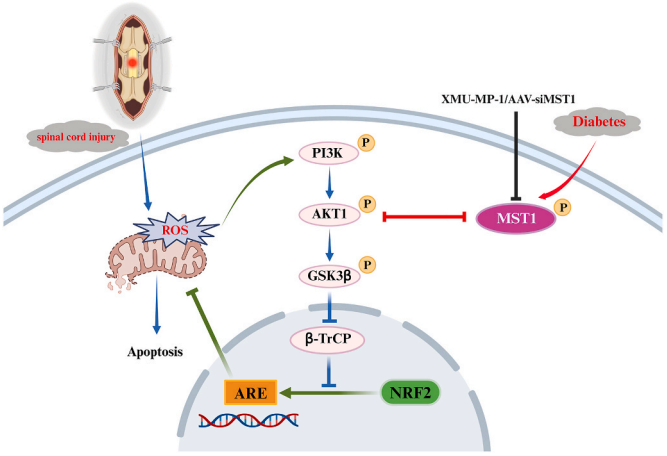

Fig. 10. Schematic summarizing the regulatory role of MST1 on neuronal apoptosis in spinal cord injury accompanied with diabetes. Under SCI conditions, large amounts of ROS are produced, which disrupt mitochondrial function. Meanwhile, PI3K/AKT1 was activated immediately to attenuate mitochondrial dysfunction via the GSK3β(Ser 9)/β-TrCP/NRF2 pathway. Nonetheless, the diabetes-mediated elevation of MST1 activity prompts NRF2 degradation by directly inhibiting AKT1 phosphorylation, aggravating neuronal apoptosis, and impeding SCI recovery.

that MST1 silencing reduced mitochondria-specific ROS levels and elevated the mitochondrial membrane potential. However, the mitochondrial protective effects were abolished by siNRF2, suggesting that NRF2 mediates the inhibition of the mitochondrial apoptotic pathway. Interestingly, our results showed that 28 days post-surgery, the protein levels for the antioxidant enzymes in the neurons were lower than those 14 days post-surgery. Two potential reasons for this were considered: (i) in an oxidative stress environment, the antioxidant components exhibited fatigue and decompensation during the chronic phase of SCI; and (ii) as the oxidative stress gradually diminishes during the chronic stage, it ceases to evoke a pronounced compensatory antioxidant response.

NRF2 regulation primarily occurs at the protein level [54]. Under normal conditions, NRF2 remains at a low basal level because of rapid proteasomal degradation following its synthesis. Emerging evidence has suggested that the stabilization and nuclear localization of NRF2 are both primarily regulated by Keap1 and β-TrCP, which are both E3 ubiquitin ligase adaptors [39]. A key finding of this study was that MST1 upregulation during hyperglycaemia did not alter the level of Keap1, indicating that MST1 negatively regulated NRF2 through Keap1-independent pathways. Previous studies have also suggested that a high-glucose environment prompts β-TrCP-mediated ubiquitination and degradation of NRF2 [31,55]; however, they did not examine the specific physiological procedures that affect neural cells. This study has also revealed that in diabetes, MST1 hyperactivity coincided with reduced AKT1 activation (phosphorylation), GSK3β activation (dephosphorylation), and decreased nuclear NRF2 protein levels. In contrast, both MST1 depletion and the MST-1 inhibitor XMU-MP-1 restored AKT1 phosphorylation and NRF2 levels. Furthermore, immunoprecipitation results indicated that under immediate oxidative conditions, NRF2 ubiquitination and degradation were reduced. The direct inhibition of AKT1 phosphorylation by MST1 was also observed in an in vitro diabetes model. By using the AKT inhibitor triciribine, GSK3β was maintained on a non-phosphorylated state, thereby facilitating subsequent β-TrCP-mediated NRF2 degradation, indicating that AKT1 may act as upstream of NRF2. In summary, the results provide solid evidence for the involvement of the AKT1/GSK3β(Ser 9)/β-TrCP signaling cascade in NRF2-mediated enhancement of antioxidants after the knockdown of MST1.

There were some limitations in this study that should be noted. The rat pheochromocytoma cell line PC12 is frequently used to mimic the neurobiology and neuropharmacology of actual neurons in vitro. Nonetheless, mature primary neurons are a better choice for studying the stress conditions in the neuronal system. Furthermore, in our study, mice with MST1 knockdown exhibited more pronounced motor function recovery than the SCI-only mice. This may be attributed not only to the sustained activation of the antioxidant capacity by MST1 knockdown but also to other relevant regulatory mechanisms that warrant further exploration.

In summary this study has revealed for the first time that MST1 inhibition significantly restores neurological function in SCI mice with preexisting diabetes, and robustly ameliorates oxidative damage in neurons, which is largely attributed to the activation of antioxidant properties via the GSK3β(Ser 9)/β-TrCP/NRF2 pathway. Collectively, our study provides evidence that MST1 could be a pharmacological target for the treatment of SCI accompanied by diabetes.

Funding statement

This work was supported by following grants: National Natural Science Foundation of China (82372400, 82072455, U22A20297, 82172433, 82102642, 81772349); Guangdong Basic and Applied Basic Research Foundation (2019A1515012181, 2023A1515010313); Guangzhou Science and Technology Project (2023A03J0203, 202102010164); The Key Research and Development Program of Guangdong Province (2019B020236002); The Key Research and Development Program of Guangzhou (202206060003).

CRediT authorship contribution statement

Weijun Huang: Writing – review & editing, Writing – original draft, Visualization, Validation, Software, Project administration, Methodology, Investigation, Formal analysis, Data curation, Conceptualization. **Depeng Wu:** Writing – review & editing, Visualization, Supervision, Software, Methodology, Investigation, Formal analysis, Conceptualization. **Chaoyang Cai:** Writing – review & editing, Validation, Software, Project administration, Methodology, Investigation, Formal analysis. **Hui Yao:** Writing – review & editing, Visualization, Supervision, Resources, Project administration, Funding acquisition, Formal analysis. **Zhenming Tian:** Visualization, Validation, Supervision, Resources, Project administration, Methodology, Conceptualization. **Yang Yang:** Writing – review & editing, Supervision, Methodology, Formal analysis, Conceptualization. **Mao Pang:** Writing – review & editing, Supervision, Resources, Project administration, Methodology, Conceptualization. **Limin Rong:** Writing – review & editing, Supervision, Resources, Project administration, Methodology, Funding acquisition, Conceptualization. **Bin Liu:** Writing – review & editing, Supervision, Resources, Project administration, Methodology, Funding acquisition, Conceptualization.

Declaration of competing interest

All authors have approved the final version of this manuscript and declared that no competing interest exists.

Data availability

Data will be made available on request.

Acknowledgements

We acknowledge and appreciate our colleagues for their valuable input and technical support for this study.

Appendix A. Supplementary data

Supplementary data to this article can be found online at https://doi.org/10.1016/j.redox.2024.103104.

References

[1] M.A. Anderson, J.W. Squair, M. Gautier, et al., Natural and targeted circuit reorganization after spinal cord injury, Nat. Neurosci. 25 (12) (2022) 1584–1596, https://doi.org/10.1038/s41593-022-01196-1.
[2] H. Cowan, C. Lakra, M. Desai, Autonomic dysreflexia in spinal cord injury, BMJ 371 (2020) m3596, https://doi.org/10.1136/bmj.m3596.
[3] A. Anjum, M.D. Yazid, M. Fauzi Daud, et al., Spinal cord injury: pathophysiology, multimolecular interactions, and underlying recovery mechanisms, Int. J. Mol. Sci. 21 (20) (2020), https://doi.org/10.3390/ijms21207533.
[4] K. Kobayakawa, H. Kumamaru, H. Saiwai, et al., Acute hyperglycemia impairs functional improvement after spinal cord injury in mice and humans, Sci. Transl. Med. 6 (256) (2014) 256ra137, https://doi.org/10.1126/scitranslmed.3009430.
[5] M. Machino, K. Ando, K. Kobayashi, et al., Risk factors for poor outcome of cervical laminoplasty: multivariate analysis in 505 patients with cervical spondylotic myelopathy, Spine 46 (5) (2021) 329–336, https://doi.org/10.1097/BRS.0000000000003783.
[6] F. Xiong, K. Gong, H. Xu, et al., Optimized integration of metabolomics and lipidomics reveals brain region-specific changes of oxidative stress and neuroinflammation in type 1 diabetic mice with cognitive decline, J. Adv. Res. 43 (2023) 233–245, https://doi.org/10.1016/j.jare.2022.02.011.
[7] W.J. Liu, H.F. Jiang, F.U. Rehman, et al., Lycium barbarum polysaccharides decrease hyperglycemia-aggravated ischemic brain injury through maintaining mitochondrial fission and fusion balance, Int. J. Biol. Sci. 13 (7) (2017) 901–910, https://doi.org/10.7150/ijbs.18404.
[8] S. Sharma, C.E. Brown, Microvascular basis of cognitive impairment in type 1 diabetes, Pharmacol. Ther. 229 (2022) 107929, https://doi.org/10.1016/j.pharmthera.2021.107929.
[9] S.L. Daly, B.J. Gabbe, R.E. Climie, C.L. Ekegren, Association between type 2 diabetes and long-term outcomes in middle-aged and older trauma patients, J. Trauma Acute Care Surg. 92 (1) (2022) 185–192, https://doi.org/10.1097/TA.0000000000003317.
[10] S. Rajan, M.J. McNeely, M. Hammond, B. Goldstein, F. Weaver, Association between obesity and diabetes mellitus in veterans with spinal cord injuries and disorders, Am. J. Phys. Med. Rehabil. 89 (5) (2010) 353–361, https://doi.org/10.1097/PHM.0b013e3181d896b9.
[11] K.S. Park, J.B. Kim, M. Keung, et al., Chronic hyperglycemia before spinal cord injury increases inflammatory reaction and astrogliosis after injury: human and rat studies, J. Neurotrauma 37 (9) (2020) 1165–1181, https://doi.org/10.1089/neu.2019.6724.
[12] K.L. Zhou, Y.F. Zhou, K. Wu, et al., Stimulation of autophagy promotes functional recovery in diabetic rats with spinal cord injury, Sci. Rep. 5 (2015) 17130, https://doi.org/10.1038/srep17130.
[13] M. Tariq, C. Morais, P.N. Kishore, N. Biary, S. Al Deeb, K. Al Moutaery, Neurological recovery in diabetic rats following spinal cord injury, J. Neurotrauma 15 (4) (1998) 239–251, https://doi.org/10.1089/neu.1998.15.239.
[14] Y.S. Lee, D.C. Cho, C.H. Kim, I. Han, E.Y. Gil, K.T. Kim, Effect of curcumin on the inflammatory reaction and functional recovery after spinal cord injury in a hyperglycemic rat model, Spine J. 19 (12) (2019) 2025–2039, https://doi.org/10.1016/j.spinee.2019.07.013.
[15] Z. Chen, H. Guo, Z. Lu, K. Sun, Q. Jin, Hyperglycemia aggravates spinal cord injury through endoplasmic reticulum stress mediated neuronal apoptosis, gliosis and activation, Biomed. Pharmacother. 112 (2019) 108672, https://doi.org/10.1016/j.biopha.2019.108672.
[16] T. Zrzavy, C. Schwaiger, I. Wimmer, et al., Acute and non-resolving inflammation associate with oxidative injury after human spinal cord injury, Brain 144 (1) (2021) 144–161, https://doi.org/10.1093/brain/awaa360.
[17] S. Zhao, J. Yin, L. Zhou, et al., Hippo/MST1 signaling mediates microglial activation following acute cerebral ischemia-reperfusion injury, Brain Behav. Immun. 55 (2016) 236–248, https://doi.org/10.1016/j.bbi.2015.12.016.
[18] L. Xiao, D. Chen, P. Hu, et al., The c-Abl-MST1 signaling pathway mediates oxidative stress-induced neuronal cell death, J. Neurosci. 31 (26) (2011) 9611–9619, https://doi.org/10.1523/JNEUROSCI.0035-11.2011.
[19] P. Zhang, T. Wang, D. Zhang, et al., Exploration of MST1-mediated secondary brain injury induced by intracerebral hemorrhage in rats via hippo signaling pathway, Transl Stroke Res 10 (6) (2019) 729–743, https://doi.org/10.1007/s12975-019-00702-1.
[20] F. Napolitano, A. Ali Adou, A. Vastola, I.F. Angelillo, Rotavirus infection and vaccination: knowledge, beliefs, and behaviors among parents in Italy, Int. J. Environ. Res. Publ. Health 16 (10) (2019), https://doi.org/10.3390/ijerph16101807.
[21] F. Yu, W. Han, G. Zhan, et al., Differential levels of hippo signaling in selected brain and peripheral tissues in streptozotocin-induced cognitive dysfunction in mice, Neuroscience 421 (2019) 48–58, https://doi.org/10.1016/j.neuroscience.2019.09.018.
[22] E.M. Ryan, P. Sadiku, P. Coelho, et al., NRF2 activation reprograms defects in oxidative metabolism to restore macrophage function in chronic obstructive pulmonary disease, Am. J. Respir. Crit. Care Med. 207 (8) (2023) 998–1011, https://doi.org/10.1164/rccm.202203-0482OC.
[23] A. Silva-Palacios, M. Ostolga-Chavarria, C. Zazueta, M. Konigsberg, Nrf2: molecular and epigenetic regulation during aging, Ageing Res. Rev. 47 (2018) 31–40, https://doi.org/10.1016/j.arr.2018.06.003.
[24] S. Bono, M. Feligioni, M. Corbo, Impaired antioxidant KEAP1-NRF2 system in amyotrophic lateral sclerosis: NRF2 activation as a potential therapeutic strategy, Mol. Neurodegener. 16 (1) (2021) 71, https://doi.org/10.1186/s13024-021-00479-8.
[25] L. Fao, S.I. Mota, A.C. Rego, Shaping the Nrf2-ARE-related pathways in Alzheimer's and Parkinson's diseases, Ageing Res. Rev. 54 (2019) 100942, https://doi.org/10.1016/j.arr.2019.100942.
[26] W. Zhao, N. Gasterich, T. Clarner, et al., Astrocytic Nrf2 expression protects spinal cord from oxidative stress following spinal cord injury in a male mouse model, J. Neuroinflammation 19 (1) (2022) 134, https://doi.org/10.1186/s12974-022-02491-1.
[27] M.H. Ge, H. Tian, L. Mao, et al., Zinc attenuates ferroptosis and promotes functional recovery in contusion spinal cord injury by activating Nrf2/GPX4 defense pathway, CNS Neurosci. Ther. 27 (9) (2021) 1023–1040, https://doi.org/10.1111/cns.13657.
[28] R. Radhakrishnan, R.A. Kowluru, Long noncoding RNA MALAT1 and regulation of the antioxidant defense system in diabetic retinopathy, Diabetes 70 (1) (2021) 227–239, https://doi.org/10.2337/db20-0375.
[29] H. Song, M. Wang, T. Xin, Mst1 contributes to nasal epithelium inflammation via augmenting oxidative stress and mitochondrial dysfunction in a manner dependent on Nrf2 inhibition, J. Cell. Physiol. 234 (12) (2019) 23774–23784, https://doi.org/10.1002/jcp.28945.
[30] Q. Zhang, X. Cheng, H. Zhang, et al., Dissecting molecular mechanisms underlying H(2)O(2)-induced apoptosis of mouse bone marrow mesenchymal stem cell: role of Mst1 inhibition, Stem Cell Res. Ther. 11 (1) (2020) 526, https://doi.org/10.1186/s13287-020-02041-7.
[31] Y. Sun, S. Zhou, H. Guo, et al., Protective effects of sulforaphane on type 2 diabetes-induced cardiomyopathy via AMPK-mediated activation of lipid metabolic pathways and NRF2 function, Metabolism 102 (2020) 154002, https://doi.org/10.1016/j.metabol.2019.154002.
[32] V. Cepas, M. Collino, J.C. Mayo, R.M. Sainz, Redox signaling and advanced glycation endproducts (AGEs) in diet-related diseases, Antioxidants 9 (2) (2020), https://doi.org/10.3390/antiox9020142.
[33] C. Michaeloudes, H. Abubakar-Waziri, R. Lakhdar, et al., Molecular mechanisms of oxidative stress in asthma, Mol. Aspect. Med. 85 (2022) 101026, https://doi.org/10.1016/j.mam.2021.101026.
[34] J. Zhang, C.M. Simpson, J. Berner, et al., Systematic identification of anticancer drug targets reveals a nucleus-to-mitochondria ROS-sensing pathway, Cell 186 (11) (2023) 2361–2379 e2325, https://doi.org/10.1016/j.cell.2023.04.026.
[35] W. Liu, P. Tang, J. Wang, et al., Extracellular vesicles derived from melatonin-preconditioned mesenchymal stem cells containing USP29 repair traumatic spinal cord injury by stabilizing NRF2, J. Pineal Res. 71 (4) (2021) e12769, https://doi.org/10.1111/jpi.12769.
[36] Q. Huang, Z. Liu, Y. Yang, et al., Selenium nanodots (SENDs) as antioxidants and antioxidant-prodrugs to rescue islet beta cells in type 2 diabetes mellitus by restoring mitophagy and alleviating endoplasmic reticulum stress, Adv. Sci. 10 (19) (2023) e2300880, https://doi.org/10.1002/advs.202300880.
[37] Y. Song, W. Ding, Y. Bei, et al., Insulin is a potential antioxidant for diabetes-associated cognitive decline via regulating Nrf2 dependent antioxidant enzymes, Biomed. Pharmacother. 104 (2018) 474–484, https://doi.org/10.1016/j.biopha.2018.04.097.
[38] P. Wang, J. Geng, J. Gao, et al., Macrophage achieves self-protection against oxidative stress-induced ageing through the Mst-Nrf2 axis, Nat. Commun. 10 (1) (2019) 755, https://doi.org/10.1038/s41467-019-08680-6.
[39] Y. Fang, B. Chen, A.Y. Gong, et al., The ketone body beta-hydroxybutyrate mitigates the senescence response of glomerular podocytes to diabetic insults, Kidney Int. 100 (5) (2021) 1037–1053, https://doi.org/10.1016/j.kint.2021.06.031.
[40] A. Mohs, T. Otto, K.M. Schneider, et al., Hepatocyte-specific NRF2 activation controls fibrogenesis and carcinogenesis in steatohepatitis, J. Hepatol. 74 (3) (2021) 638–648, https://doi.org/10.1016/j.jhep.2020.09.037.
[41] R. Fernandez-Gines, J.A. Encinar, J.D. Hayes, et al., Corrigendum to "An inhibitor of interaction between the transcription factor NRF2 and the E3 ubiquitin ligase adapter beta-TrCP delivers anti-inflammatory responses in mouse liver" [Redox

Biol. 55 (2022) 102396/PMID: 35839629], Redox Biol. 55 (2022) 102428, https://doi.org/10.1016/j.redox.2022.102428.
[42] H.K. Bryan, A. Olayanju, C.E. Goldring, B.K. Park, The Nrf2 cell defence pathway: Keap1-dependent and -independent mechanisms of regulation, Biochem. Pharmacol. 85 (6) (2013) 705–717, https://doi.org/10.1016/j.bcp.2012.11.016.
[43] A. Ardestani, F. Paroni, Z. Azizi, et al., MST1 is a key regulator of beta cell apoptosis and dysfunction in diabetes, Nat. Med. 20 (4) (2014) 385–397, https://doi.org/10.1038/nm.3482.
[44] B. Cinar, P.K. Fang, M. Lutchman, et al., The pro-apoptotic kinase Mst1 and its caspase cleavage products are direct inhibitors of Akt1, EMBO J. 26 (21) (2007) 4523–4534, https://doi.org/10.1038/sj.emboj.7601872.
[45] G. Pekkurnaz, X. Wang, Mitochondrial heterogeneity and homeostasis through the lens of a neuron, Nat. Metab. 4 (7) (2022) 802–812, https://doi.org/10.1038/s42255-022-00594-w.
[46] K.C. Luk, Oxidative stress and alpha-synuclein conspire in vulnerable neurons to promote Parkinson's disease progression, J. Clin. Invest. 129 (9) (2019) 3530–3531, https://doi.org/10.1172/JCI130351.
[47] E.H. Ahn, K. Lei, S.S. Kang, et al., Mitochondrial dysfunction triggers the pathogenesis of Parkinson's disease in neuronal C/EBPbeta transgenic mice, Mol. Psychiatr. 26 (12) (2021) 7838–7850, https://doi.org/10.1038/s41380-021-01284-x.
[48] M. Khan, B.P.F. Rutten, M.O. Kim, MST1 regulates neuronal cell death via JNK/Casp 3 signaling pathway in HFD mouse brain and HT22 cells, Int. J. Mol. Sci. 20 (10) (2019), https://doi.org/10.3390/ijms20102504.
[49] A. Cuadrado, Structural and functional characterization of Nrf2 degradation by glycogen synthase kinase 3/beta-TrCP, Free Radic. Biol. Med. 88 (Pt B) (2015) 147–157, https://doi.org/10.1016/j.freeradbiomed.2015.04.029.
[50] D. Martin, M. Salinas, N. Fujita, T. Tsuruo, A. Cuadrado, Ceramide and reactive oxygen species generated by H2O2 induce caspase-3-independent degradation of Akt/protein kinase B, J. Biol. Chem. 277 (45) (2002) 42943–42952, https://doi.org/10.1074/jbc.M201070200.
[51] Z. Xiong, Y. Li, Z. Zhao, et al., Mst1 knockdown alleviates cardiac lipotoxicity and inhibits the development of diabetic cardiomyopathy in db/db mice, Biochim. Biophys. Acta, Mol. Basis Dis. 1866 (8) (2020) 165806, https://doi.org/10.1016/j.bbadis.2020.165806.
[52] S. Zhang, J. Zhao, M. Wu, et al., Over-activation of TRPM2 ion channel accelerates blood-spinal cord barrier destruction in diabetes combined with spinal cord injury rat, Int. J. Biol. Sci. 19 (8) (2023) 2475–2494, https://doi.org/10.7150/ijbs.80672.
[53] M. George, M. Tharakan, J. Culberson, A.P. Reddy, P.H. Reddy, Role of Nrf2 in aging, Alzheimer's and other neurodegenerative diseases, Ageing Res. Rev. 82 (2022) 101756, https://doi.org/10.1016/j.arr.2022.101756.
[54] E. Crisman, P. Duarte, E. Dauden, et al., KEAP1-NRF2 protein-protein interaction inhibitors: design, pharmacological properties and therapeutic potential, Med. Res. Rev. 43 (1) (2023) 237–287, https://doi.org/10.1002/med.21925.
[55] S. Zhou, P. Wang, Y. Qiao, et al., Genetic and pharmacologic targeting of glycogen synthase kinase 3 beta reinforces the Nrf2 antioxidant defense against podocytopathy, J. Am. Soc. Nephrol. 27 (8) (2016) 2289–2308, https://doi.org/10.1681/ASN.2015050565.